
Pipeline Gradient-based Model Training on Analog In-memory Accelerators

Zhaoxian Wu

Rensselaer Polytechnic Institute
Troy, NY 12180
wuz16@rpi.edu

Quan Xiao

Rensselaer Polytechnic Institute
Troy, NY 12180
xiaoq5@rpi.edu

Tayfun Gokmen

IBM T. J. Watson Research Center
Yorktown Heights, NY 10598
tgokmen@us.ibm.com

Hsinyu Tsai

IBM T. J. Watson Research Center
Yorktown Heights, NY 10598
htsai@us.ibm.com

Kaoutar El Maghraoui

IBM T. J. Watson Research Center
Yorktown Heights, NY 10598
kelmaghr@us.ibm.com

Tianyi Chen

Rensselaer Polytechnic Institute
Troy, NY 12180
chentianyi19@gmail.com*

Abstract

Aiming to accelerate the training of large deep neural models in an energy-efficient way, an analog in-memory computing (AIMC) accelerator emerges as a solution with immense potential. In AIMC accelerators, trainable weights are kept in memory without the need to move from memory to processors during the training, significantly reducing overhead. However, although the in-memory feature enables efficient computation, it also constrains the use of data parallelism since copying weights from one AIMC to another is expensive. To enable parallel training using AIMC, we propose synchronous and asynchronous pipeline parallelism for AIMC accelerators inspired by the pipeline in digital domains. This paper provides a theoretical convergence guarantee for both synchronous and asynchronous pipelines in terms of both sampling and clock cycle complexity, which is non-trivial since the physical characteristic of AIMC accelerators leads to analog updates that suffer from asymmetric bias. The simulations of training deep models on real datasets verify the efficiency of pipeline analog training.

1 Introduction

Deep Neural Networks (DNNs) have facilitated remarkable progress in a wide range of applications. As the model sizes and dataset volumes grow exponentially, DNN training and inference become time-consuming and resource-intensive. For example, it requires 184 thousand GPU hours to train an LLAMA2 7 billion model, and this time increases to 1.7 million GPU hours for its 70 billion version [1]. Stemming from the escalating computational demands of large-scale DNN training and inference, the pursuit of specialized hardware accelerators emerges. In principle, ideal specialized hardware for DNN should be efficient, support large-scale parallelism, and remain lower energy-economic simultaneously. As the demand for efficient processing intensifies, the fundamental backbone of both

*The work was supported by National Science Foundation (NSF) project 2412486, NSF CAREER project 2047177, and the IBM-Rensselaer Future of Computing Research Collaboration.

training and inference largely relies on matrix-vector multiplication (MVM) operation, which is the core component of the ubiquitous fully connected and convolutional layers. Typically, each forward and backward pass requires on the order of millions of multiply-accumulate (MAC) operations, necessitating specialized hardware with high performance and low energy consumption.

The promise of analog computing. To this end, a promising solution to accelerate the MVM operations is the *analog in-memory computing* (AIMC) accelerator, wherein both the input and output of MVM operation are analog signals, and the trainable weights of DNN layers are stored in analog crossbar tiles [2]. Different from traditional Von Neumann accelerators like GPU and TPU, which require weight movement from memory to processor before computation, the AIMC accelerator keeps the weight stationary and performs MVM operations in memory. Without moving weights frequently, AIMC accelerators enable time- and energy-efficient MVM computations; see Figure 1.

The curse of data parallelism. While efficient computation is a benefit, in-memory computing imposes limitations on scalability. Specifically, contemporary DNN optimizers depend on mini-batch SGD to facilitate highly parallel training. In the Von Neumann computation architecture, the most efficient parallel mechanism is *data parallelism* [3], where DNN weights are replicated to different computation devices to support gradient descent with large batches [4, 5]. On the contrary, in AIMC architecture, the trainable weights are stored in the analog tiles in the form of device conductances, and thus, copying weights from one analog tile to another is expensive and prone to error. Therefore, data parallelism, the enabling factor of large-scale AI training, is unrealistic for AIMC accelerators.

Due to the physical limitations of the AIMC accelerator, we instead resort to *pipeline parallelism* [6], another prevalent parallel mechanism. In pipeline parallelism, a large model is partitioned into a series of smaller stages and gets distributed across multiple devices, with each stage corresponding to the computation of a few layers. After a device finishes the process of one datum (or one batch), it passes the intermediate outputs to the next devices and begins the process of the next data. In this way, the model that is too large to fit into one device can be separated into different AIMC devices, enlarging the efficient memory. Meanwhile, the computation on different devices can happen simultaneously, and the systems can process more data in a given period of time.

While pipelining is a simple idea, implementing it in analog training faces a series of crucial challenges. First, AIMC accelerators usually suffer from noisy gradient signals and asymmetric updates [7, 8], which introduce errors on all forward, backward, and update passes. Second, to fully realize the potential of pipeline parallelism, the weight update pass usually involves stale gradients. Both of them incur errors in the training, leading to the following question:

How to design analog pipeline parallel training approaches that do not impair the training?

This paper answers this question by analyzing the sample complexity of different pipeline algorithms and wall-clock time. Before that, we will briefly review prior work that attempted to solve the issues.

Gradient-based training on AIMC accelerators. Analog SGD implemented by pulse update is extremely efficient [8]. However, the asymmetric update and noisy gradient lead to large asymptotic errors in training [7]. To overcome these issues, a family of analog training algorithms, Tiki-Taka (TT) has been proposed. TT-v1 [9] heuristically introduces an auxiliary analog array as a gradient approximation to eliminate the asymptotic error. To demonstrate its efficiency, [10] establishes a model to characterize the dynamic of the analog training and provides a theoretical convergence guarantee. To filter out the high-frequency noise introduced by inter-device transfer, TT-v2 [11] introduces a digital array. Based on TT-v1/v2, Chopped-TTv2 (c-TTv2) and Analog Gradient Accumulation with Dynamic reference (AGAD) [12] are proposed to mitigate the impact of inaccurate symmetric point correction [13]. Despite the above efforts, analog training of large models on huge datasets is still a major challenge.

Synchronous and asynchronous parallelism. Typically, existing pipeline designs can be classified into two categories. If the weights are updated using the latest gradients, it is *synchronous* pipeline; otherwise, it is *asynchronous* pipeline. As the computing requirement of training large models emerges, a plethora of pipeline parallel libraries has been developed, including Gpipe [14, 15], Deepspeed [16], FSDP [17], Megetron-LM [18], Colossal-AI [19], just to name a few. Nevertheless, they are synchronous pipeline that enjoys the same dynamic as SGD, so they have the same convergence guarantee as SGD. Apart from that, researchers also made some effort to explore the asynchronous pipeline. For instance, [20] studied the asynchronous pipeline setting and proposed weight-prediction approaches to compensate for the delay. PipeDream [21] combined the synchronous and asyn-

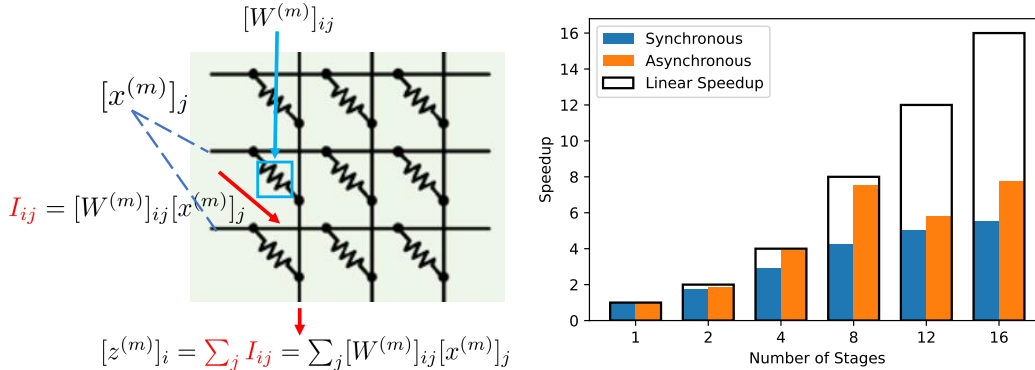


Figure 1: **(Left)** Illustration of MVM computation in AIMC accelerators. The **weight** $W^{(m)}$ on layer m is stored in a crossbar tile consisting of an array of resistors. The (i, j) -th element of $W^{(m)}$ is represented by the **conductance** of the (i, j) -th resistor. To perform an MVM operation $z^{(m)} = W^{(m)}x^{(m)}$, **voltage** $[x^{(m)}]_j$ is applied between j -th and $(j + 1)$ -th row. By Ohm’s law, the **current** is $I_{ij} = [W^{(m)}]_{ij}[x^{(m)}]_j$; and by Kirchoff’s law, the total current on the i -th column is $\sum_j I_{ij} = \sum_j [W^{(m)}]_{ij}[x^{(m)}]_j$. Unlike the digital counterpart, no movement of $W^{(m)}$ is required. **(Right)** Speedup of the proposed pipeline training methods as the number of stages increases compared with single machine training case (stage=1); see Section 5 for more details.

chronous pipeline parallelisms to achieve greater speedup. To mitigate the negative effect of stale gradients, [22] and [23] have proposed only overlapping gradient computation and communication so that delay is always one. However, these algorithms are *not for analog pipeline training*. Researchers also attempted to design analog pipeline circuits to accelerate the training [24, 25], but they focus on the synchronous pipeline. On the theory side, there are a few studies on pipeline training on digital devices such as [26], but these results rely on weight stashing, which is *expensive for analog accelerators*. As [21] points out, delay affects both forward and backward passes in the asynchronous pipeline training. It renders the increment no longer a valid gradient without the weight stashing and makes the analysis challenging.

In the context of prior work, we summarize our key contributions as follows.

- C1) To fully embrace the promise of analog computing, we systematically study the pipeline training on AIMC accelerators, which enables training larger models by distributing models across multiple accelerators and increasing computation density. We study the existing work and classify them as synchronous pipelines, which achieve considerable speedup, but their computation density is still sub-optimal. To further increase the computation density, we propose the *first* asynchronous pipeline training algorithm on AIMC accelerators.
- C2) We provide a convergence guarantee for the proposed algorithms. Theoretical results show that two strategies have pros and cons: synchronous pipeline has a better complexity while its computation density in the device is lower; asynchronous pipeline reduces device idleness but involves stale gradients. The main results are summarized in Table 1.
- C3) We conduct empirical simulation to demonstrate the efficiency of pipeline training. The results show that both pipeline algorithms significantly outperform their non-pipeline counterparts. Despite a slightly larger sample complexity, the asynchronous pipeline achieves the same accuracy with fewer clock cycles because of its high computation density. Furthermore, the asynchronous pipeline achieves linear-speedup at least within the range of 1-8 devices; see Figure 1.

2 Model Training on AIMC Accelerators

In this section, we first introduce the generic gradient-based training algorithm, encompassing digital algorithms running on devices like GPU and TPU, and algorithms running on AIMC accelerators.

Pipeline Type	Sample Comp.	Comp. Density	Clock Cycle
w.o. Pipeline	$O(\sigma^2 \varepsilon^{-2})$	$\frac{1}{M}$	$O(M\sigma^2 \varepsilon^{-2})$
Synchronous [Theorem 1]	$O(\sigma^2 \varepsilon^{-2})$	$\frac{1}{M+B-1}$	$O((M+B)B^{-1}\sigma^2 \varepsilon^{-2})$
Asynchronous [Theorem 2]	$O(\sigma^2 \varepsilon^{-2} + \varepsilon^{-1})$	1	$O(\sigma^2 \varepsilon^{-2} + \varepsilon^{-1})$

Table 1: Comparison of different pipeline strategies. Sample complexity (Sample Comp.) is the number of samples needed for achieving training loss $\leq \varepsilon$. Computation density (Comp. Density) is the time that is the portion of time when the system is computing the gradients. In the table, M is the pipeline depth, and B is the micro-batch size. Clock Cycle measures the running time for achieving training loss $\leq \varepsilon$, which in math is sample complexity divided by clock cycle.

Consider a standard model training problem on a data distribution \mathcal{D} , given by

$$W^* := \arg \min_{W \in \mathbb{R}^D} f(W) \quad \text{with} \quad f(W) := \mathbb{E}_{\xi \sim \mathcal{D}} [f(W; \xi)] \quad (1)$$

where W is all trainable weights of the model vectorized into a D dimensional vector.

DNN model. Consider the multi-layer DNN, which consists only of linear layers and activation functions. Let $[M] := \{1, 2, \dots, M\}$ denote a positive integer set. The trainable weights are separated into M different blocks, i.e., $W = [W^{(1)}, W^{(2)}, \dots, W^{(M)}]$, where $W^{(m)}, \forall m \in [M]$ is a matrix. The training of DNN typically consists of three phases: forward, backward, and update. Suppose x and y are the feature and label of data $\xi = (x, y) \in \mathcal{X} \times \mathcal{Y}$, where \mathcal{X} and \mathcal{Y} are feature and label space, respectively. The forward pass of the model for layer $m \in [M]$ can be expressed by

$$\text{Forward} \quad x^{(1)} = x, \quad z^{(m)} = W^{(m)}x^{(m)}, \quad x^{(m+1)} = g^{(m)}(z^{(m)}) \quad (2)$$

where $g^{(m)}$ is the activation function of layer m , and $x^{(M)}$ is the feature from the last layer, which is fed together with label y into the loss function $\ell(\cdot, \cdot) : \mathcal{Y} \times \mathcal{Y} \rightarrow \mathbb{R}$ and yields $f(W; \xi) = \ell(x^{(M+1)}, y)$. For the backward pass, define the backward error $\delta^{(m)} := \frac{\partial f(W; \xi)}{\partial z^{(m)}}$, wherein the error of last layer is first computed by $\delta^{(M)} = \nabla_{x^{(M+1)}} \ell(x^{(M+1)}, y) \nabla g^{(M)}(z^{(M)})$. Subsequently, each layer $m \in [M-1]$ computes the next recursion according to

$$\text{Backward} \quad \delta^{(m)} = \frac{\partial f(W; \xi)}{\partial z^{(m+1)}} \frac{\partial z^{(m+1)}}{\partial x^{(m+1)}} \frac{\partial x^{(m+1)}}{\partial z^{(m)}} = (\delta^{(m+1)} W^{(m)}) \nabla g^{(m)}(z^{(m)}). \quad (3)$$

In the forward pass, the activation $z^{(m)}$ is stashed until the backward signal $\delta^{(m+1)}$ returns. Typically, the computation $\nabla g^{(m)}(z)$ is light-weight, and hence the major overhead of the backward pass lies at the MVM among W and δ . With the forward and backward signals, the gradient with respect to the weight $W^{(m)}$ of layer m is computed by

$$\text{Gradient} \quad \nabla_{W^{(m)}} f(W; \xi) = \frac{\partial f(W; \xi)}{\partial z^{(m)}} \frac{\partial z^{(m)}}{\partial W^{(m)}} = \delta^{(m)} \otimes x^{(m)} \quad (4)$$

where \otimes is the outer product between two vectors. Having the gradients of each layer, we can use different gradient-based algorithms to update the weights.

Gradient-based training on AIMC accelerators. After getting the backward signal $\delta^{(m)}$, gradient-based algorithms can be used to update the weights. In digital devices, one of the most popular training algorithms is stochastic gradient descent (SGD), wherein the matrix $\nabla_{W^{(m)}} f(W; \xi) = \delta^{(m)} \otimes x^{(m)}$ is computed and added to $W_k^{(m)}$, written by $W_{k+1}^{(m)} = W_k^{(m)} - \alpha \nabla_{W^{(m)}} f(W_k; \xi_k)$; $\alpha > 0$ is a positive learning rate. In the paper, the subscript k is used to indicate the index of gradient update.

Different from digital devices, AIMC accelerator uses *rank-update* to update the gradient update, which constructs a series of pulses and sends them to its analog array [8]. Without computing the whole matrix $\delta^{(m)} \otimes x^{(m)}$ explicitly, AIMC accelerators perform the update operation in a fast and energy-efficient way. Nevertheless, rank-update relies on the special structure that the gradient of $W_k^{(m)}$ is a rank-one matrix, which brings us further challenges.

On top of that, as existing work pointed out [9, 10], the update on AIMC accelerators suffers from asymmetric bias, and thus the dynamic of Analog SGD in single-machine training can be written as

$$W_{k+1}^{(m)} = W_k^{(m)} - \alpha \nabla_{W^{(m)}} f(W_k; \xi_k) - \frac{\alpha}{\tau} |\nabla_{W^{(m)}} f(W_k; \xi_k)| \odot W_k^{(m)} \quad (5)$$

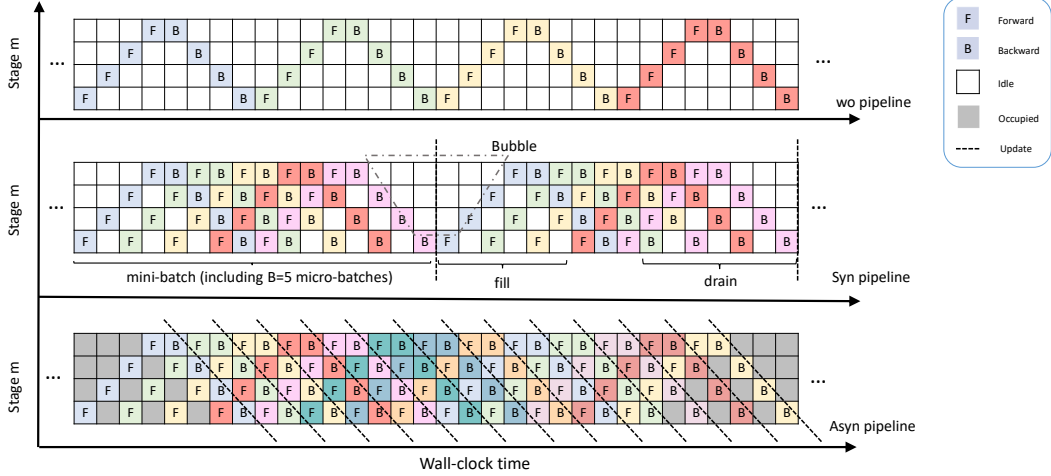


Figure 2: Illustration of pipelines with 4 devices ($M = 4$). Each mini-batch is split into $B = 4$ micro-batches. Each color represents one micro-batch, and each row from bottom to top represents stages 0 to 4. Each column corresponds to a clock cycle in which one micro-batch is processed. The white square indicates the idle device. **(Top)** Vanilla model parallelism without pipeline. All weights are updated using gradient-based algorithms after the computation of one mini-batch is completed, which is not presented in the figure. **(Middle)** Synchronous pipeline with micro-batch count $B = 5$. The update happens after all 5 micro-batches are processed. **(Bottom)** Asynchronous pipeline. The update happens once the gradient of one micro-batch is achieved. The grey square indicates the corresponding device is processing data that is not fully reflected in the figure.

where τ is a device-dependent constant. When $\tau \rightarrow \infty$, Analog SGD reduces to Digital SGD.

The main challenge coming from the asymmetric is the *saturation phenomenon* [9]. Consider the update of (i, j) -th element of matrix $W_k^{(m)}$, whose update is written as

$$\begin{aligned}
 ([W_{k+1}^{(m)}]_{ij} - [W_k^{(m)}]_{ij})^2 &= \alpha^2 (\text{sign}([\nabla_{W^{(m)}} f(W_k; \xi_k)]_{ij}) - [W_k^{(m)}]_{ij}/\tau)^2 (\nabla_{W^{(m)}} f(W_k; \xi_k))^2 \\
 &\approx 0 \quad \text{if } [W_k^{(m)}]_{ij} \approx \tau \text{sign}([\nabla_{W^{(m)}} f(W_k; \xi_k)]_{ij})
 \end{aligned} \tag{6}$$

which means that the increment is suppressed when $[W_k^{(m)}]_{ij}$ gets close to the τ . Therefore, we usually introduce a proper scaling coefficient so that the saturation never happens during the training.

3 Analog Pipeline Model Training

This section introduces pipeline parallelism and shows how it increases computational efficiency.

Consider training a large model using a mini-batch size B_{mini} , which is too large to fit into one device and motivates us to adopt *model parallelism*. In model parallelism, the computation is partitioned into a sequence of *stages*, which, in general, consists of a consecutive set of layers in the model. Each stage is mapped on one digital or analog device. For simplicity, we assume each stage contains one layer only. Apart from the model separation, a mini-batch of data is also split into B *micro-batch* of size $B_{\text{micro}} := B_{\text{mini}}/B$. For simplicity, let the micro-batch size $B_{\text{micro}} = 1$ in Sections 3-4 so that the subscript b in $\xi_{k,b}$ can represent the index of micro-batch or data, and $B = B_{\text{mini}}$ can represent the number of micro-batch and mini-batch size B_{mini} . It could be easily extended to general cases.

Clock cycle. We define the maximum time for each stage to process one micro-batch as the *clock cycle*. Ideally, all devices would process a micro-batch in the same amount of time, avoiding idle periods during a clock cycle. Although achieving this is challenging, various task scheduling approaches have been proposed to balance computation [21, 14]. To explore the potential of pipeline training, this paper uses the clock cycle and stage as the minimal time and basic scheduling units, respectively. Based on scheduling methods, there are three types of model parallelism: vanilla model parallelism without pipelining, synchronous pipelining, and asynchronous pipelining.

Model parallelism without pipeline. Let $\xi_{k,b}, b \in [B]$ denote the b -th micro-batch (containing only one data, as previously mentioned) for iteration k . Vanilla model parallelism processes all micro-batches one by one. In the forward pass, stage m achieves the output of the previous stage $x_{k,b}^{(m)}$ as

input and outputs $x_{k,b}^{(m+1)}$, while stage m achieves the backward error $\delta_{k,b}^{(m)}$ from next stage and sends the error $\delta_{k,b}^{(m-1)}$ to its previous stage in the backward pass. The signals $x_{k,b}^{(m)}$ and $\delta_{k,b}^{(m)}$ are stored when the gradient for the b -th micro-batch is completed. After achieving all $\{(x_{k,b}^{(m)}, \delta_{k,b}^{(m)}) : b \in [B_{\text{mini}}]\}$, the weights will be updated using the gradient-based method. Beginning from $W_{k,0} = W_k$, Analog SGD update the weight as $W_{k+1}^{(m)} = W_{k,B}$, which iterates over $b \in [B_{\text{mini}}]$ by

$$W_{k,b+1}^{(m)} = W_{k,b}^{(m)} - \frac{\alpha}{B} \nabla_{W^{(m)}} f(W_k; \xi_{k,b}) - \frac{\alpha}{\tau B} |\nabla_{W^{(m)}} f(W_k; \xi_{k,b})| \odot W_{k,b}^{(m)}. \quad (7)$$

Notice that for digital SGD, the last term in the right-hand side (RHS) of (7) disappears, and hence (7) reduces to mini-batch SGD, i.e., $W_{k+1}^{(m)} = W_k^{(m)} - \frac{\alpha}{B} \sum_{b=1}^B \nabla_{W^{(m)}} f(W_k; \xi_{k,b})$. However, for the AIMC accelerators, only rank-update is permitted so that each gradient is accumulated to the weight $W_k^{(m)}$ one by one, rendering the analysis more difficult.

Synchronous pipeline. Existing work has already attempted to design architecture that supports the pipeline training [24, 25]. They faithfully implement the iteration (7) and overlap parts of the computation. Since they compute all gradients in a batch on the same W_k , their algorithms can be called *synchronous pipeline*. In the vanilla non-pipeline version, the stage m is idle after its forward computation of b -th micro-batch until the backward error comes back from stage $m + 1$. In the synchronous pipeline training, each stage sends the output signal $x_{k,b}^{(m+1)}$ to the next stage, while simultaneously starting to process the next forward signal $x_{k,b+1}^{(m)}$ or backward signal $\delta_{k,b-(M-m)}^{(m)}$, if any; see the middle of Figure 2. Similar to the vanilla non-pipeline version, the weights will be updated after processing all micro-batches. To implement that, a synchronization operation is required to wait for the completion of gradient computation before starting the next mini-batch (fill and drain periods), hence rendering some devices idle.

Asynchronous pipeline. To increase the usage of all devices, a more progressive strategy, asynchronous pipeline, is proposed. Instead of waiting for the gradient of one mini-batch, the asynchronous pipeline training method performs gradient-based update algorithms immediately after one micro-batch is completed. Except for short periods of fill and drain at the beginning and the end, all devices are active during the training, maximizing the training efficiency; see the bottom of Figure 2.

Despite its perfect resource usage, asynchronous pipeline parallelism suffers from the stale signal issue. Notice that in the asynchronous pipeline setting, the forward signal $x^{(m)}$ and backward signals $\delta^{(m)}$ are computed based on different stale weights. For example, after outputting forward signal $x^{(0)}$ for the k -th micro-batch, the first stage ($m = 1$) receives the backward signal $\delta^{(0)}$ after $2(M - 1)$ clock cycles, wherein $M - 1$ gradient updates happen. Consequently, the gradient is stale for the current weights. Furthermore, notice both forward (2) and backward (3) passes involve the matrix $W^{(m)}$ while the $W^{(m)}$ is changed between the forward and backward passes. To depict the process more precisely, we introduce different symbols, which have tildes on top of them to indicate the staleness. Since the mini-batch is no longer needed in asynchronous pipeline, the subscript b for the micro-batch index can be omitted, and we denote the micro-batch for k -th update as ξ_k . To make the relationship clearer, the computation dependency is plotted in Figure 3.

Since there are $M - m$ gradient updates between the forward and backward passes in stage m , the weight used for the forward pass has a delay of $M - m$, that is

$$\tilde{x}_k^{(m+1)} = g^{(m)}(\tilde{z}_k^{(m)}), \quad \tilde{z}_k^{(m)} = W_{k-(M-m)}^{(m)} \tilde{x}_k^{(m)}, \quad \tilde{x}_k^{(0)} = x_k. \quad (8)$$

In contrast, the weights are updated following the backward pass, which means the weight used for backward is the latest one

$$\tilde{\delta}_k^{(m)} = \tilde{\delta}_k^{(m+1)} W_k^{(m+1)} \nabla g^{(m)}(\tilde{z}_k^{(m)}), \quad (9)$$

$$W_{k+1}^{(m)} = W_k^{(m)} - \alpha \tilde{\delta}_k^{(m)} \otimes \tilde{x}_k^{(m)} - \frac{\alpha}{\tau} |\tilde{\delta}_k^{(m)} \otimes \tilde{x}_k^{(m)}| \odot W_k^{(m)}. \quad (10)$$

In (10), the outer product $\tilde{\delta}_k^{(m)} \otimes \tilde{x}_k^{(m)}$ is no longer a valid gradient with respect to any weight $W^{(m)}$, which is referred to as *partial delay gradient*, making the analysis more challenging.

Remark 1 (Digital v.s. analog asynchronous pipeline). *In digital hardware, one can stash the stale weight $W_{k-(M-m)}^{(m)}$ and read it out again to compute the backward signal in (9) [26, 21]. Weight*

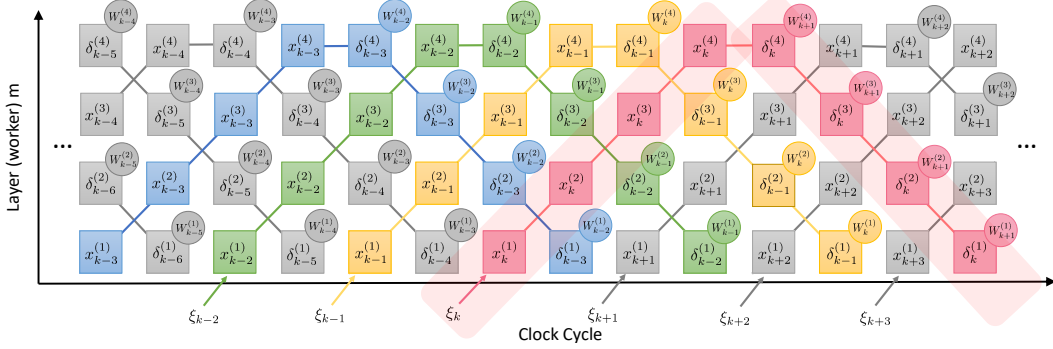


Figure 3: Illustration of the dynamic of asynchronous pipeline. The $W_k^{(m)}$ in the circle implies the update happens in this clock cycle, and the symbols in the squares indicate the input of each device.

stashing ensures the outer product $\tilde{\delta}_k^{(m)} \otimes \tilde{x}_k^{(m)}$ is the gradient with respect to $W_{k-(M-m)}^{(m)}$, and hence provides a better convergence guarantee. However, copying is expensive in the analog domain, as we discussed before. Consequently, the asynchronous pipeline suffers from partial delay gradient issues.

Computation density. Different pipeline strategies can process varying amounts of data in the same amount of time. In an ideal scenario, a micro-batch requires $2M$ clock cycles for forward and backward passes, distributed equally across M devices, taking 2 clock cycles per micro-batch. To measure how closely an algorithm approaches this ideal, we introduce *computation density*. Let $N_c(t)$ be the number of data points processed in t clock cycles. Assuming infinite runtime, we define computation density as the limit ratio of ideal processing time to real time: $\lim_{t \rightarrow \infty} \frac{2N_c(t)}{t}$, where we introduce the factor 2 since each data involves forward and backward passes. For vanilla model parallelism without pipelining, it takes $2M$ cycles per micro-batch, yielding a computation density of $1/M$. In synchronous pipelining, it takes $2(M+B-1)$ clock cycles to process B micro-batches, resulting in a density of $B/(M+B-1)$. Asynchronous pipelining achieves a density of 1, as all devices remain active during training.

4 Convergence and Wall-clock Analysis

This section provides the convergence guarantee of the proposed pipeline training algorithm on AIMC accelerators. We show that both synchronous and asynchronous pipelines enjoy the same convergence rate as the vanilla non-pipeline version. By increasing the computation density significantly, the pipeline parallelism provides notable speedup in terms of clock cycle complexity.

4.1 Assumptions on models, data, and AIMC accelerators

Before showing the complexity of the pipeline algorithms, we first introduce a series of assumptions on the properties of DNN structures, data distribution, as well as the AIMC accelerators. Unless stated otherwise, $\|\cdot\|$ is ℓ_2 -norm for vectors and Frobenius norm for matrices.

Assumption 1 (Unbiasness and bounded variance). *The sample ξ_k are independently sampled from a distribution \mathcal{D} over times $k \in [K]$, and has bounded variance, i.e., $\mathbb{E}_{\xi_k}[\nabla f(W_k; \xi_k)] = \nabla f(W_k)$ and $\mathbb{E}_{\xi_k}[\|\nabla f(W_k; \xi_k) - \nabla f(W_k)\|^2] \leq \sigma^2$.*

Assumption 2 (Normalized feature). *The feature is normalized, i.e. $\|x\| = 1, \forall x \in \mathcal{X}$.*

Assumption 3 (Activation function). *All activation function $g^{(m)}(\cdot)$, $m \in [M]$, is (i) Lipschitz continuous, i.e. $\|g^{(m)}(z) - g^{(m)}(z')\| \leq L_{g,0}\|z - z'\|$; (ii) smooth, i.e. $\|\nabla g^{(m)}(z) - \nabla g^{(m)}(z')\| \leq L_{g,1}\|z - z'\|$; (iii) centered, i.e. $g(0) = 0$.*

The conditions (i) and (ii) in Assumption 3 hold for many activation functions like Sigmoid and Tanh functions, while (iii) can be achieved by adding an offset mapping before the activation function if there is a point x such that $g(x) = 0$.

Assumption 4 (Loss function). *The loss $\ell(\cdot, \cdot)$ is smooth with respect to the first input, i.e. $\|\nabla_1 \ell(y_1, y) - \nabla_1 \ell(y_2, y)\| \leq L_{\ell,1}\|y_1 - y_2\|, \forall y_1, y_2, y$; lower bounded, i.e. $\ell(y_1, y_2) \geq f^*, \forall y_1, y_2$.*

Note that the lower bounded loss implies the lower boundness of the objectives as well, i.e. $f(W; \xi) \geq f^*$, $\forall W \in \mathbb{R}^D, x \in \mathcal{X}$. Aside from the assumptions, to avoid saturation during training, we also need proper scaling so that the saturation degree of the AIMC accelerators is bounded.

Assumption 5 (Bounded Saturation). *There exists a positive constant $W_{\max} < \tau$ such that all the weight $W_k^{(m)}$, $m \in [M]$ is ℓ_∞ norm bounded, i.e., $\|W_k^{(m)}\|_\infty \leq W_{\max} < \tau, \forall k \in [K]$. The ratio W_{\max}/τ is referred to as saturation degree.*

Assumption 5 requires the AIMC accelerators to have a sufficiently large active region to represent weights. Besides, on digital devices, the trainable weights always remain bounded in a small neighborhood of the initialization points during training [27–29], especially for overparameterized networks. Given W_{\max} is sufficiently large to include this neighborhood, Assumption 5 holds. While it is possible to prove this assumption, we adopt it to make our results more concise and to focus on revealing the key insights on the effect of pipeline training.

Under the above assumptions, we prove the objective $f(W; \xi)$ is smooth.

Lemma 1 (smoothness of the objective). *Under Assumption 2–5, the objective is L_f -smooth with respect to W , i.e. $\forall \xi = (x, y), \|\nabla f(W; \xi) - \nabla f(\tilde{W}; \xi)\| \leq L_f \|W - \tilde{W}\|$.*

The proof of Lemma 1 is deferred to Appendix C. Lemma 1 enables us to adapt the tools from [30] for our analysis. However, due to the asymmetric bias of the AIMC accelerators, the convergence results for Analog SGD are still non-trivial.

4.2 Convergence rate of pipeline training algorithms

In this section, we provide the convergence rate of Analog SGD with pipelines. In non-convex optimization tasks like the DNN training, instead of measuring the objective (1), it is more common to measure the gradient square norm $\|\nabla f(W_k)\|^2$.

Theorem 1 (Convergence rate, synchronous pipeline). *Under Assumption 1–5, if the learning rate is set as $\alpha = \sqrt{\frac{B(f(W_0) - f^*)}{\sigma^2 L_f K}}$ and K is sufficiently large such that $\alpha \leq \frac{1}{L_f}$, it holds that*

$$\frac{1}{K} \sum_{k=0}^{K-1} \mathbb{E}[\|\nabla f(W_k)\|^2] \leq 4\sqrt{\frac{(f(W_0) - f^*)\sigma^2 L_f}{BK}} \frac{1}{1 - W_{\max}^2/\tau^2} + \sigma^2 S$$

where S denotes the amplification factor given by $S := \frac{W_{\max}/\tau^2}{1 - W_{\max}^2/\tau^2}$.

The proof of Theorem 1 is deferred to Appendix D. Similar to the convergence of digital SGD [30], Analog SGD converges in the rate $O(\sqrt{\sigma^2/(BK)})$. However, because of the asymmetric bias, the convergence rate slows down by a factor $\frac{1}{1 - W_{\max}^2/\tau^2}$, which reduces to 1 when τ tends to infinity.

Besides, the asymmetric bias introduces an additional term $\sigma^2 S$, which is independent of K and hence referred to as *asymptotic error*. When the AIMC accelerators can be well-designed, τ can be sufficiently large, and it does not dominate the error when K . Empirically, researchers also proposed some Analog SGD variants like Tiki-Taka [9, 11] to eliminate the negative impact of asymmetric bias. Next, we provide the iteration complexity of Analog SGD with asynchronous pipeline training.

Theorem 2 (Convergence rate, asynchronous pipeline). *Under Assumption 1–5, if the learning rate is set as $\alpha = \sqrt{\frac{f(W_0) - f^*}{\sigma^2 L_f K}}$ and K is sufficiently large such that $\alpha \leq \frac{1}{L_f}$, it holds that*

$$\frac{1}{K} \sum_{k=0}^{K-1} \mathbb{E}[\|\nabla f(W_k)\|^2] \leq 4\sqrt{\frac{(f(W_0) - f^*)\sigma^2 L_f}{K}} \frac{1}{1 - (1+u)W_{\max}^2/\tau^2} + \sigma^2 S' + O\left(\frac{1+1/u}{K}\right)$$

where $u > 0$ is any number and S' denotes the amplification factor given by $S' := \frac{(1+u)W_{\max}^2/\tau^2}{1 - (1+u)W_{\max}^2/\tau^2}$.

The proof of Theorem 2 is deferred to Appendix E. Because of the stale signals, the convergence rate of the asynchronous pipeline slows down. The coefficient of the dominant term degrades from $\frac{1}{1 - W_{\max}^2/\tau^2}$ to $\frac{1}{1 - (1+u)W_{\max}^2/\tau^2}$, and an extra error term $O\left(\frac{1+1/u}{K}\right)$ is introduced. Fortunately, $O\left(\frac{1+1/u}{K}\right)$ is not the dominant term and we can specify u as a small constant so the impact is minor.

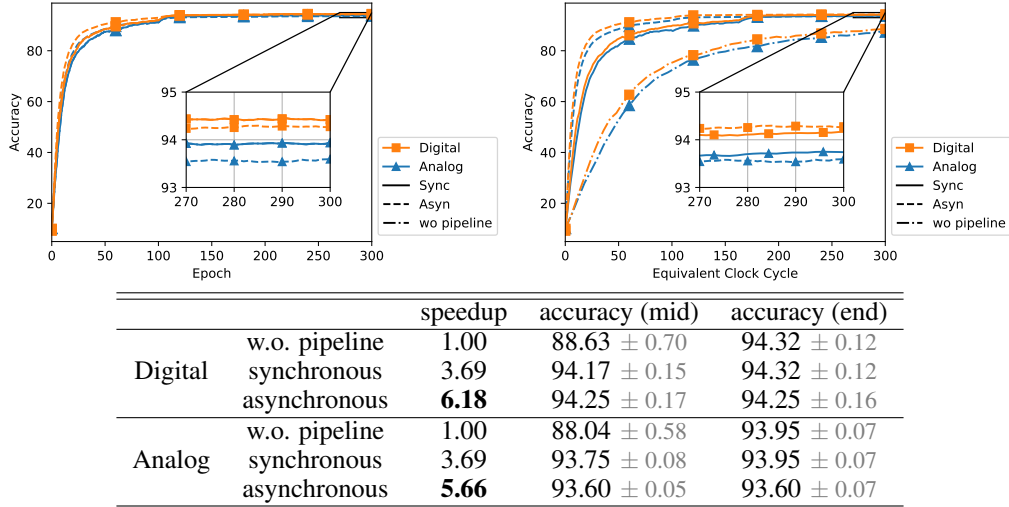


Figure 4: Training ResNet10 on CIFAR10 dataset via vanilla model parallelism without pipeline (wo pipeline), synchronous pipeline (Sync), and asynchronous pipeline (Asyn). **(Left)** Accuracy-vs-Epoch reflects sample complexity. **(Right)** Accuracy-vs-Clock cycle. **(Bottom)** Speedup and test accuracy. The speedup is computed by comparing the clock cycle to reach 93% accuracy. The test accuracy and standard deviation at clock cycle 300 (mid) and epoch 300 (end) are reported.

Remark 2. For digital SGD with the synchronous pipeline training, the convergence rate is given in [30]. We also provide the convergence analysis for SGD with asynchronous pipeline training on digital devices, detailed in Theorem 2 in the Appendix F. Unlike analog training, both synchronous and asynchronous pipeline training do not slow down digital SGD.

4.3 Sampling complexity and clock cycle complexity

The convergence rate alone does not indicate the total training time, as different algorithms require varying numbers of gradient updates. The bottleneck during a micro-batch process is the forward and backward computations, which depend on the number of micro-batches. Thus, we focus on the sample complexity of the algorithms, defined as the minimal gradient computation needed to achieve the desired error. Due to the existence of asymptotic error, we define the sample complexity of synchronous and asynchronous pipelines as the minimum micro-batch needed for achieving $\frac{1}{K} \sum_{k=0}^{K-1} \mathbb{E} [\|\nabla f(W_k)\|^2] \leq \varepsilon + E$, where E is the asymptotic error, i.e. $\sigma^2 S$ for vanilla model parallelism without pipeline/synchronous pipeline and $\sigma^2 S'$ for asynchronous pipeline, respectively. Noticing that the former requires B micro-batches at each iteration while the latter requires 1, and omitting the constant $\frac{1}{1-W_{\max}^2/\tau^2}$ or $\frac{1}{1-(1+u)W_{\max}^2/\tau^2}$, we have the following corollary.

Corollary 1 (Sample complexity). *The sample complexities of model parallelism without pipeline and synchronous pipeline are $O(\sigma^2 \varepsilon^{-2})$, while that of the asynchronous pipeline is $O(\sigma^2 \varepsilon^{-2} + \varepsilon^{-1})$.*

Corollary 1 claims that three model parallelisms share the same dominant term $O(\sigma^2 \varepsilon^{-2})$ in the sample complexity, while asynchronous pipeline slows down by a factor and a non-dominant term $O(\varepsilon^{-1})$. Dividing the sample complexity by the computation density, we know the number of clock cycles they need to achieve the ε accuracy.

Corollary 2 (Clock cycle complexity). *The clock cycle complexities of vanilla model parallelism without pipeline, synchronous pipeline, and asynchronous pipeline are $O(M\sigma^2 \varepsilon^{-2})$, $O((M+B-1)B^{-1}\sigma^2 \varepsilon^{-2})$, and $O(\sigma^2 \varepsilon^{-2} + \varepsilon^{-1})$, respectively.*

The results are summarized in Table 1. By overlapping the computation among micro-batches, synchronous pipeline achieves M times acceleration compared to its non-pipeline counterpart without any cost. Asynchronous pipeline overlaps more computation, achieving higher computation density with slight scarification of convergence rate. When the mini-batch is split into sufficient micro-batch so that $B \gg M$, the bubble time can be omitted, and synchronous pipeline achieves the best clock cycle complexity. However, when the number of micro-batch is small, the asynchronous pipeline is able to achieve better acceleration.

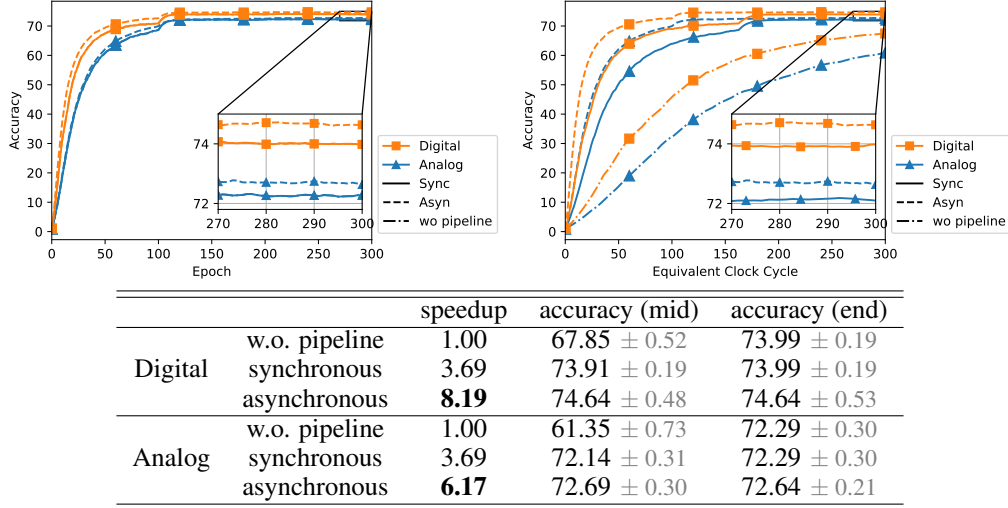


Figure 5: Training ResNet10 on CIFAR100 dataset via vanilla model parallelism without pipeline (wo pipeline), synchronous pipeline (Sync), and asynchronous pipeline (Asyn). **(Left)** Accuracy-vs-Epoch reflects sample complexity. **(Right)** Accuracy-vs-Clock cycle. **(Bottom)** Speedup and test accuracy. The speedup is computed by comparing the clock cycle to reach 72% accuracy. The test accuracy and standard deviation at clock cycle 300 (mid) and epoch 300 (end) are reported.

5 Numerical Simulations

In this section, we test our methods in an open-source IBM Analog Hardware Acceleration Kit (AIHWKIT) [31]; see github.com/IBM/aihwkit. In the simulations, we train a ResNet10 to perform an image classification task on CIFAR10 and CIFAR100 datasets; see Figure 4 and 5. The network consists of $M = 6$ stages, consisting 1 convolution layer, 4 residual blocks, and 1 fully-connected layer. We map the first 5 stages on digital devices and the last one onto an AIMC (analog) device. We use digital SGD, implemented by PYTORCH library. The pipeline parallelism is also simulated on a single GPU. To get the *equivalent clock cycle* in the figures, we map the epoch to the clock cycle by dividing the computation density, as discussed in Section 3. Each simulation is repeated three times, and the mean and standard deviation are reported. More details are reported in Appendix G.

Sample complexity and clock cycle complexity. The results in the left of Figure 4 show that the accuracy-epoch curves of all three pipeline strategies almost overlap with each other, implying all of these algorithms have the same sample complexity. We fit the mini-batch size as $B_{\text{mini}} = 128$ and micro-batch size as $B_{\text{micro}} = 16$. It can be seen that synchronous pipeline training accelerates convergence to the target accuracy with a speedup of over $3\times$ on both digital and analog devices compared to the non-pipeline training. Asynchronous pipeline training achieves an even greater speedup, $6\times \sim 8\times$, which is greater than the theoretical prediction $\times M = \times 6$. We conjecture that it happens because the generalization benefits from the delay property of asynchronous pipeline [32].

Effect of micro-batch size. We also report the effect of micro-batch sizes in Table 2. We fit the mini-batch size as $B_{\text{mini}} = 128$ and change the micro-batch size. For synchronous pipeline training, increasing the batch size improves the speedup on both digital and analog devices. Moreover, asynchronous pipeline training consistently results in higher speedup compared to the synchronous version. The trade-off is that the asynchronous pipeline sacrifices the accuracy and can only reach lower accuracy when the training time is sufficiently long.

Effect of stage/device number. We extensively explored the impact of increasing device count on the speedup achieved through pipeline parallelism; see Figure 1. In the simulations, we train Resnet34 model on CIFAR10 dataset, which could be separated into $M = 1, 2, 4, 8, 12, 16$ stages. Assuming the model can be evenly divided into multiple stages, and the equivalent clock cycle needed to compute the entire model is fixed. The results reveal that the asynchronous pipeline achieves linear-speedup at least within the range of 1-8 devices. Even though some latency, like communication latency, are ignored in the simulations, the comparison is still fair since the asynchronous pipeline does not introduce obvious extra latency.

	B_{micro}	Synchronous			Asynchronous		
		speedup	acc (mid)	acc (end)	speedup	acc (mid)	acc (end)
D	16	3.69			6.18	94.25 \pm 0.17	94.25 \pm 0.16
	32	2.67			6.06	94.27 \pm 0.18	94.28 \pm 0.20
	64	1.71	94.17 \pm 0.15	94.32 \pm 0.12	6.00	94.09 \pm 0.13	94.08 \pm 0.15
	128	1.00			5.83	93.68 \pm 0.39	93.67 \pm 0.38
A	16	3.69	93.75 \pm 0.08	93.95 \pm 0.07	5.66	93.60 \pm 0.05	93.60 \pm 0.07
	32	2.67	93.57 \pm 0.12	93.95 \pm 0.07	5.88	93.62 \pm 0.13	93.61 \pm 0.11
	64	1.71	90.86 \pm 0.44	93.95 \pm 0.07	5.88	93.58 \pm 0.14	93.60 \pm 0.17
	128	1.00	88.04 \pm 0.58	93.95 \pm 0.07	4.89	93.36 \pm 0.06	93.37 \pm 0.06

Table 2: The training of Resnet10 model on CIFAR10 dataset. The test accuracy and standard deviation under different micro-batch sizes at clock cycle 300 (mid) and epoch 300 (end). The speedup is computed by comparing the clock cycle needed to reach 93% target accuracy. The accuracy of synchronous is not affected by micro-batch size.

6 Conclusions and Limitations

This paper study the pipeline algorithms for AIMC accelerators in the convergence and computation aspects. We study the existing synchronous pipeline algorithm and propose the first asynchronous pipeline algorithm on AIMC accelerators. The synchronous pipeline achieves the best convergence rate in terms of sample complexity, but training bubbles reduce computation density. To enable more devices to be active, an asynchronous pipeline discards the synchronization at the end of one mini-batch, achieving a higher computation density, with the cost of slightly increased sample complexity. Simulations reveal the extraordinary speedup potential of our asynchronous pipeline for analog computing. A limitation of this work is that AIMC accelerator behaviors can only be simulated but not on the actual analog chips. But this is a necessary step for every new technology, and future work should verify its efficiency as the technology matures.

References

- [1] Hugo Touvron, Louis Martin, Kevin Stone, Peter Albert, Amjad Almahairi, Yasmine Babaei, Nikolay Bashlykov, Soumya Batra, Prajwal Bhargava, Shruti Bhosale, et al. Llama 2: Open foundation and fine-tuned chat models. *arXiv preprint arXiv:2307.09288*, 2023.
- [2] Shubham Jain et al. Neural network accelerator design with resistive crossbars: Opportunities and challenges. *IBM Journal of Research and Development*, 63(6):10–1, 2019.
- [3] Shen Li, Yanli Zhao, Rohan Varma, Omkar Salpekar, Pieter Noordhuis, Teng Li, Adam Paszke, Jeff Smith, Brian Vaughan, Pritam Damania, et al. Pytorch distributed: Experiences on accelerating data parallel training. *arXiv preprint arXiv:2006.15704*, 2020.
- [4] Priya Goyal, Piotr Dollár, Ross Girshick, Pieter Noordhuis, Lukasz Wesolowski, Aapo Kyrola, Andrew Tulloch, Yangqing Jia, and Kaiming He. Accurate, large minibatch SGD: Training Imagenet in 1 hour. *arXiv preprint arXiv:1706.02677*, 2017.
- [5] Yang You, Jing Li, Sashank Reddi, Jonathan Hseu, Sanjiv Kumar, Srinadh Bhojanapalli, Xiaodan Song, James Demmel, Kurt Keutzer, and Cho-Jui Hsieh. Large batch optimization for deep learning: Training BERT in 76 minutes. In *International Conference on Learning Representations*, 2020.
- [6] Weizheng Xu, Youtao Zhang, and Xulong Tang. Parallelizing DNN training on GPUs: Challenges and opportunities. In *Companion Proceedings of the Web Conference*, pages 174–178, 2021.
- [7] Geoffrey W Burr, Robert M Shelby, Severin Sidler, Carmelo Di Nolfo, Junwoo Jang, Irem Boybat, Rohit S Shenoy, Pritish Narayanan, Kumar Virwani, Emanuele U Giacometti, et al. Experimental demonstration and tolerancing of a large-scale neural network (165 000 synapses) using phase-change memory as the synaptic weight element. *IEEE Transactions on Electron Devices*, 62(11):3498–3507, 2015.

- [8] Tayfun Gokmen and Yurii Vlasov. Acceleration of deep neural network training with resistive cross-point devices: Design considerations. *Frontiers in neuroscience*, 10:333, 2016.
- [9] Tayfun Gokmen and Wilfried Haensch. Algorithm for training neural networks on resistive device arrays. *Frontiers in Neuroscience*, 14, 2020.
- [10] Zhaoxian Wu, Tayfun Gokmen, Malte J Rasch, and Tianyi Chen. Towards exact gradient-based training on analog in-memory computing. *Advances in Neural Information Processing Systems*, 2024.
- [11] Tayfun Gokmen. Enabling training of neural networks on noisy hardware. *Frontiers in Artificial Intelligence*, 4:1–14, 2021.
- [12] Malte J Rasch, Fabio Carta, Omebayode Fagbohunge, and Tayfun Gokmen. Fast offset corrected in-memory training. *arXiv preprint arXiv:2303.04721*, 2023.
- [13] Murat Onen, Tayfun Gokmen, Teodor K Todorov, Tomasz Nowicki, Jesús A Del Alamo, John Rozen, Wilfried Haensch, and Seyoung Kim. Neural network training with asymmetric crosspoint elements. *Frontiers in artificial intelligence*, 5, 2022.
- [14] Yanping Huang, Youlong Cheng, Ankur Bapna, Orhan Firat, Dehao Chen, Mia Chen, HyoukJoong Lee, Jiquan Ngiam, Quoc V Le, Yonghui Wu, et al. Gpipe: Efficient training of giant neural networks using pipeline parallelism. *Advances in neural information processing systems*, 32, 2019.
- [15] Chiheon Kim, Heungsub Lee, Myungryong Jeong, Woonhyuk Baek, Boogeon Yoon, Ildoo Kim, Sungbin Lim, and Sungwoong Kim. torchgpipe: On-the-fly pipeline parallelism for training giant models. *arXiv preprint arXiv:2004.09910*, 2020.
- [16] Jie Ren, Samyam Rajbhandari, Reza Yazdani Aminabadi, Olatunji Ruwase, Shuangyan Yang, Minjia Zhang, Dong Li, and Yuxiong He. Zero-offload: Democratizing billion-scale model training. In *USENIX Annual Technical Conference*, pages 551–564, 2021.
- [17] Yanli Zhao, Andrew Gu, Rohan Varma, Liang Luo, Chien-Chin Huang, Min Xu, Less Wright, Hamid Shojanazeri, Myle Ott, Sam Shleifer, et al. Pytorch FSDP: experiences on scaling fully sharded data parallel. *arXiv preprint arXiv:2304.11277*, 2023.
- [18] Mohammad Shoeybi, Mostofa Patwary, Raul Puri, Patrick LeGresley, Jared Casper, and Bryan Catanzaro. Megatron-lm: Training multi-billion parameter language models using model parallelism. *arXiv preprint arXiv:1909.08053*, 2019.
- [19] Shenggui Li, Hongxin Liu, Zhengda Bian, Jiarui Fang, Haichen Huang, Yuliang Liu, Boxiang Wang, and Yang You. Colossal-AI: A unified deep learning system for large-scale parallel training. In *International Conference on Parallel Processing*, pages 766–775, 2023.
- [20] Atli Kosson, Vitaliy Chiley, Abhinav Venigalla, Joel Hestness, and Urs Koster. Pipelined backpropagation at scale: training large models without batches. *Proceedings of Machine Learning and Systems*, 3:479–501, 2021.
- [21] Deepak Narayanan, Aaron Harlap, Amar Phanishayee, Vivek Seshadri, Nikhil R Devanur, Gregory R Ganger, Phillip B Gibbons, and Matei Zaharia. Pipedream: generalized pipeline parallelism for DNN training. In *Proceedings of the 27th ACM symposium on operating systems principles*, pages 1–15, 2019.
- [22] Yangrui Chen, Cong Xie, Meng Ma, Juncheng Gu, Yanghua Peng, Haibin Lin, Chuan Wu, and Yibo Zhu. SAPIpe: Staleness-aware pipeline for data parallel DNN training. *Advances in Neural Information Processing Systems*, 35:17981–17993, 2022.
- [23] Youjie Li, Mingchao Yu, Songze Li, Salman Avestimehr, Nam Sung Kim, and Alexander Schwing. Pipe-SGD: A decentralized pipelined SGD framework for distributed deep net training. *Advances in Neural Information Processing Systems*, 31, 2018.

- [24] Ali Shafiee, Anirban Nag, Naveen Muralimanohar, Rajeev Balasubramonian, John Paul Strachan, Miao Hu, R Stanley Williams, and Vivek Srikumar. ISAAC: A convolutional neural network accelerator with in-situ analog arithmetic in crossbars. *ACM SIGARCH Computer Architecture News*, 44(3):14–26, 2016.
- [25] Linghao Song, Xuehai Qian, Hai Li, and Yiran Chen. Pipelayer: A pipelined ReRAM-based accelerator for deep learning. In *2017 IEEE international symposium on high performance computer architecture (HPCA)*, pages 541–552. IEEE, 2017.
- [26] Zhouyuan Huo, Bin Gu, Heng Huang, et al. Decoupled parallel backpropagation with convergence guarantee. In *International Conference on Machine Learning*, pages 2098–2106. PMLR, 2018.
- [27] Samet Oymak and Mahdi Soltanolkotabi. Overparameterized nonlinear learning: Gradient descent takes the shortest path? In *International Conference on Machine Learning*, pages 4951–4960. PMLR, 2019.
- [28] Chaoyue Liu, Libin Zhu, and Mikhail Belkin. Loss landscapes and optimization in over-parameterized non-linear systems and neural networks. *Applied and Computational Harmonic Analysis*, 59:85–116, 2022.
- [29] Difan Zou and Quanquan Gu. An improved analysis of training over-parameterized deep neural networks. *Advances in neural information processing systems*, 32, 2019.
- [30] Leon Bottou, Frank Curtis, and Jorge Nocedal. Optimization Methods for Large-Scale Machine Learning. *SIAM Review*, 60(2), 2018.
- [31] Malte J Rasch, Diego Moreda, Tayfun Gokmen, Manuel Le Gallo, Fabio Carta, Cindy Goldberg, Kaoutar El Maghraoui, Abu Sebastian, and Vijay Narayanan. A flexible and fast PyTorch toolkit for simulating training and inference on analog crossbar arrays. *IEEE International Conference on Artificial Intelligence Circuits and Systems*, pages 1–4, 2021.
- [32] Xiaoge Deng, Li Shen, Shengwei Li, Tao Sun, Dongsheng Li, and Dacheng Tao. Towards understanding the generalizability of delayed stochastic gradient descent. *arXiv preprint arXiv:2308.09430*, 2023.
- [33] Tayfun Gokmen, Murat Onen, and Wilfried Haensch. Training deep convolutional neural networks with resistive cross-point devices. *Frontiers in neuroscience*, 11:538, 2017.
- [34] Ekin D Cubuk, Barret Zoph, Dandelion Mane, Vijay Vasudevan, and Quoc V Le. Autoaugment: Learning augmentation policies from data. *arXiv preprint arXiv:1805.09501*, 2018.

Supplementary Material for “Pipeline Gradient-based Model Training on Analog In-memory Accelerator”

Table of Contents

A Analog pipeline SGD from worker and data perspectives	14
B Bounds of delay errors	14
C Smoothness of the object	19
D Proof of Theorem 1: Analog SGD with synchronous pipeline	23
E Proof of Theorem 2: Analog SGD with asynchronous pipeline	24
F Convergence of digital asynchronous pipeline SGD	28
G Simulation details	30

A Analog pipeline SGD from worker and data perspectives

Involving multiple devices and data at each time step, pipeline algorithms, especially asynchronous pipeline, are usually hard to figure out. To facilitate the understanding, we list the Analog SGD under two different perspectives. In *worker perspective*, we pay more attention to how worker m processes a flow of data; see Algorithm 1. In *data perspective*, we focus on how a sample ξ_k flows through each worker; see Algorithm 2.

Algorithm 1 Analog SGD with asynchronous pipeline (Worker Perspective)

- 1: **for** iteration $k = 0, 1, 2, \dots, K$ **do**
 // Periphery device (worker 0) at the beginning
 - 2: Sample $\xi_k = (x_k, y_k)$ and Send $x_k^{(0)} = x_k$ to worker 1
 // Worker $m = 1, 2, \dots, M$ in parallel
 - 3: Receive input $\tilde{x}_k^{(m)}$ from worker $m - 1$
 - 4: Compute $\tilde{z}_k^{(m)} = W_{k-(M-m)}^{(m)} \tilde{x}_k^{(m)}$
 - 5: Compute $\tilde{x}_k^{(m+1)} = g^{(m)}(\tilde{z}_k^{(m)})$ and $\nabla g^{(m)}(\tilde{z}_k^{(m)})$
 - 6: Store input $\tilde{x}_k^{(m)}$ and $\nabla g^{(m)}(\tilde{z}_k^{(m)})$
 - 7: Receive backward error $\tilde{\delta}_{k-(M-m)}^{(m+1)}$
 - 8: $\tilde{\delta}_k^{(m)} = \tilde{\delta}_{k-(M-m)}^{(m+1)} W_k^{(m+1)} \nabla g^{(m)}(\tilde{z}_k^{(m)})$
 - 9: $W_{k+1}^{(m)} = W_k^{(m)} - \alpha \tilde{\delta}_k^{(m)} \otimes \tilde{x}_k^{(m)} - \frac{\alpha}{\tau} |\tilde{\delta}_k^{(m)} \otimes \tilde{x}_k^{(m)}| \odot W_k^{(m)}$
 // Periphery device at the end
 - 10: Compute $\tilde{\delta}_k^{(M)} = \nabla_{\tilde{x}^{(M+1)}} \ell(\tilde{x}^{(M+1)}, y_k) \nabla g^{(M)}(\tilde{z}^{(M)})$
 - 11: Send $\tilde{\delta}_k^{(M)}$ back to worker M
 - 12: **end for**
-

B Bounds of delay errors

In the asynchronous pipeline, the computations of both forward and backward passes involve stale weights, which induces delay error on the signals. This section provides a series of the bounds of the delay error.

Algorithm 2 Analog SGD with asynchronous pipeline (Data Perspective)

```

1: for iteration  $k = 0, 1, 2, \dots, K$  do
2:   Sample  $\xi_k = (x_k, y_k)$ ,  $x_k^{(0)} = x_k$ 
3:   for all worker  $m = 1, 2, \dots, M$  do
4:     Compute  $\tilde{z}_k^{(m)} = W_{k-(M-m)}^{(m)} \tilde{x}_k^{(m)}$ 
5:     Compute  $\tilde{x}_k^{(m+1)} = g^{(m)}(\tilde{z}_k^{(m)})$  and  $\nabla g^{(m)}(\tilde{z}_k^{(m)})$ 
6:   end for
7:   Compute  $\tilde{\delta}_k^{(M)} = \nabla_{\tilde{x}^{(M+1)}} \ell(\tilde{x}^{(M+1)}, y_k) \nabla g^{(M)}(\tilde{z}^{(M)})$ 
8:   for all layer  $m = M, M-1, \dots, 1$  do
9:      $\tilde{\delta}_k^{(m)} = \tilde{\delta}_k^{(m+1)} W_k^{(m+1)} \nabla g^{(m)}(\tilde{z}_k^{(m)})$ 
10:     $W_{k+1}^{(m)} = W_k^{(m)} - \alpha \tilde{\delta}_k^{(m)} \otimes \tilde{x}_k^{(m)} - \frac{\alpha}{\tau} |\tilde{\delta}_k^{(m)} \otimes \tilde{x}_k^{(m)}| \odot W_k^{(m)}$ 
11:   end for
12: end for

```

Lemma 2 (Lipschitz continuity of loss function). *There exists $L_{\ell,0}$ such that for any $m \in [M]$, $\|\nabla_{x^{(m)}} \ell(x_k^{(m)}, y_k)\| \leq L_{\ell,0}$ and $\|\nabla_{\tilde{x}^{(m)}} \ell(\tilde{x}_k^{(m)}, y_k)\| \leq L_{\ell,0}$.*

Proof. According to norm equivalence, there exists $W_{\max,2} = cW_{\max}$ with c is defined by the dimension of $W_k^{(m)}$, such that $\|W_k^{(m)}\| \leq W_{\max,2}$. For $m \in [M]$, according to the forward recursion (2), it holds that

$$\begin{aligned} \|x_k^{(m+1)}\| &\stackrel{(a)}{=} \|g^{(m)}(z_k^{(m)}) - g^{(m)}(0)\| \stackrel{(b)}{\leq} L_{g,0} \|z_k^{(m)}\| = L_{g,0} \|W_k^{(m)} x_k^{(m)}\| \\ &\leq L_{g,0} \|W_k^{(m)}\| \|x_k^{(m)}\| \leq L_{g,0} W_{\max,2} \|x_k^{(m)}\| \end{aligned} \quad (11)$$

where (a) and (b) hold because of Assumption 3 (1) and (2). Then by induction, we get $\|x_k^{(m)}\| \leq (L_{g,0} W_{\max,2})^m$ and the same bound holds for $\|x_k^{(m)}\|$. Since $\ell(\cdot, \cdot)$ is differentiable so that $\nabla \ell(\cdot, \cdot)$ is continuous, then there exists $L_{f,0}$ such that $\|\nabla_{x^{(m)}} \ell(x_k^{(m)}, y^k)\| \leq L_{f,0}$ and $\|\nabla_{\tilde{x}^{(m)}} \ell(\tilde{x}_k^{(m)}, y^k)\| \leq L_{f,0}$ hold for any $k, m \in [M]$. \square

Lemma 3 (boundeds signal). *Under Assumption 2–4, both forward and backward signals are bounded, i.e., $\forall m \in [M+1]$*

$$\|x_k^{(m)}\| \leq (L_{g,0} W_{\max,2})^m, \quad \|\delta_k^{(m)}\| \leq (L_{g,0} W_{\max,2})^{M-m} L_{\ell,0} L_{g,0}, \quad (12)$$

$$\|\tilde{x}_k^{(m)}\| \leq (L_{g,0} W_{\max,2})^m, \quad \|\tilde{\delta}_k^{(m)}\| \leq (L_{g,0} W_{\max,2})^{M-m} L_{\ell,0} L_{g,0}. \quad (13)$$

Proof of Lemma 3. This lemma is proved by induction over m . The statement for $\|x_k^{(m)}\|$ and $\|\tilde{x}_k^{(m)}\|$ at $m = 1$ trivially hold because $x_k^{(0)} = \tilde{x}_k^{(0)} = x_k$. For $\|\delta_k^{(M+1)}\|$ and $\|\tilde{\delta}_k^{(M+1)}\|$, we have

$$\begin{aligned} \|\delta_k^{(M+1)}\| &= \|\nabla_{x^{(M+1)}} \ell(x_k^{(M+1)}, y_k) \nabla g^{(M)}(z_k^{(M)})\| \\ &\leq \|\nabla_{x^{(M+1)}} \ell(x_k^{(M+1)}, y_k)\| \|\nabla g^{(M)}(z_k^{(M)})\| \leq L_{\ell,0} L_{g,0} \end{aligned} \quad (14)$$

$$\begin{aligned} \|\tilde{\delta}_k^{(M+1)}\| &= \|\nabla_{x^{(M+1)}} \ell(\tilde{x}_k^{(M+1)}, y_k) \nabla g^{(M)}(\tilde{z}_k^{(M)})\| \\ &\leq \|\nabla_{x^{(M+1)}} \ell(\tilde{x}_k^{(M+1)}, y_k)\| \|\nabla g^{(M)}(\tilde{z}_k^{(M)})\| \leq L_{\ell,0} L_{g,0}. \end{aligned} \quad (15)$$

For $m \in [M]$, according to the forward recursion (2), it holds that

$$\begin{aligned} \|x_k^{(m+1)}\| &\stackrel{(a)}{=} \|g^{(m)}(z_k^{(m)}) - g^{(m)}(0)\| \stackrel{(b)}{\leq} L_{g,0} \|z_k^{(m)}\| = L_{g,0} \|W_k^{(m)} x_k^{(m)}\| \\ &\leq L_{g,0} \|W_k^{(m)}\| \|x_k^{(m)}\| \leq L_{g,0} W_{\max,2} \|x_k^{(m)}\| \end{aligned} \quad (16)$$

where (a) and (b) hold because of Assumption 3 (1) and (2). According to the backward recursion (3), it holds that

$$\begin{aligned} \|\delta_k^{(m)}\| &= \|\delta_k^{(m+1)} W_k^{(m+1)} \nabla g^{(m)}(z_k^{(m)})\| \\ &\leq \|\delta_k^{(m+1)}\| \|W_k^{(m+1)}\| \|\nabla g^{(m)}(z_k^{(m)})\| \leq L_{g,0} W_{\max,2} \|\delta_k^{(m+1)}\|, \end{aligned} \quad (17)$$

$$\begin{aligned} \|\tilde{\delta}_k^{(m)}\| &= \|\tilde{\delta}_k^{(m+1)} W_k^{(m+1)} \nabla g^{(m)}(\tilde{z}_k^{(m)})\|, \\ &\leq \|\tilde{\delta}_k^{(m+1)}\| \|W_k^{(m+1)}\| \|\nabla g^{(m)}(\tilde{z}_k^{(m)})\| \leq L_{g,0} W_{\max,2} \|\tilde{\delta}_k^{(m+1)}\|. \end{aligned} \quad (18)$$

The proof has finished. \square

We first bound the error of the stale variables. Define $\Delta_k^{(m)} := W_{k+1}^{(m)} - W_k^{(m)}$, which is the different between consecutive weights.

Lemma 4 (Delay error of signals). *Under Assumption 2–4, the difference between the latest and stale signals are bounded, i.e., $\forall m \in [M+1]$*

$$\|\tilde{x}_k^{(m)} - x_k^{(m)}\| \leq C_x^{(m)} \sum_{m'=1}^{m-1} \sum_{k'=k-(M-m'+1)}^{k-1} \|\Delta_{k'}^{(m')}\|, \quad (19)$$

$$\|\tilde{z}_k^{(m-1)} - z_k^{(m)}\| \leq C_z^{(m)} \sum_{m'=1}^m \sum_{k'=k-(M-m'+1)}^{k-1} \|\Delta_{k'}^{(m')}\|, \quad (20)$$

$$\|\tilde{\delta}_k^{(m)} - \delta_k^{(m)}\| \leq C_\delta^{(m)} \sum_{m'=1}^M \sum_{k'=k-(M-m'+1)}^{k-1} \|\Delta_{k'}^{(m')}\|, \quad (21)$$

where the constants above are defined by

$$C_x^{(m)} := L_{g,0} (L_{g,0} W_{\max,2})^{m-1}, \quad (22)$$

$$C_z^{(m)} := (L_{g,0} W_{\max,2})^{m-1}, \quad (23)$$

$$\begin{aligned} C_\delta^{(m)} &:= (L_{g,0} W_{\max,2})^{M-m+1} (L_{\ell,1} L_{g,0}^2 + L_{\ell,0} L_{g,1}) (L_{g,0} W_{\max,2})^{M-1} \\ &\quad + (L_{g,0} W_{\max,2})^{M-1} L_{\ell,0} L_{g,1} \frac{1 - (L_{g,0} W_{\max,2})^{M-m}}{1 - L_{g,0} W_{\max,2}}. \end{aligned} \quad (24)$$

Proof of Lemma 4. We first bound the delay of forward signal $\tilde{x}_k^{(m)}$. At the first layer, there is no delay, i.e. $\tilde{x}_k^{(1)} = x_k^{(1)} = x_k$. For other layers $m > 1$

$$\begin{aligned} \|\tilde{x}_k^{(m+1)} - x_k^{(m+1)}\| &\leq L_{g,0} \|\tilde{z}_k^{(m)} - z_k^{(m)}\| \\ &= L_{g,0} \|W_{k-(M-m)}^{(m)} \tilde{x}_k^{(m)} - W_k^{(m)} x_k^{(m)}\| \\ &= L_{g,0} \|(W_{k-(M-m)}^{(m)} - W_k^{(m)}) \tilde{x}_k^{(m)} + W_k^{(m)} (\tilde{x}_k^{(m)} - x_k^{(m)})\| \\ &\stackrel{(a)}{\leq} L_{g,0} (\|W_{k-(M-m)}^{(m)} - W_k^{(m)}\|_2 \|\tilde{x}_k^{(m)}\| + \|W_k^{(m)}\|_2 \|\tilde{x}_k^{(m)} - x_k^{(m)}\|) \\ &\leq L_{g,0} ((L_{g,0} W_{\max,2})^m \|W_{k-(M-m)}^{(m)} - W_k^{(m)}\| + W_{\max,2} \|\tilde{x}_k^{(m)} - x_k^{(m)}\|) \end{aligned} \quad (25)$$

where (a) follows the triangle inequality and the consistence of ℓ_2 -matrix norm, i.e. $\|Wu\| \leq \|W\|_2 \|u\|$ where W and u are arbitrary matrix and vector, respectively. Using triangle inequality over the first term of RHS in (25), we have

$$\|W_{k-(M-m)}^{(m)} - W_k^{(m)}\| \leq \sum_{k'=k-(M-m)}^{k-1} \|W_{k'+1}^{(m)} - W_{k'}^{(m)}\| = \sum_{k'=k-(M-m)}^{k-1} \|\Delta_{k'}^{(m)}\| \quad (26)$$

and consequently,

$$\|\tilde{x}_k^{(m+1)} - x_k^{(m+1)}\| \quad (27)$$

$$\leq L_{g,0}(L_{g,0}W_{\max,2})^m \sum_{k'=k-(M-m)}^{k-1} \|\Delta_{k'}^{(m)}\| + L_{g,0}W_{\max,2}\|\tilde{x}_k^{(m)} - x_k^{(m)}\|.$$

Expanding inequality (27) from m to 1 and using the fact $\tilde{x}_k^{(1)} = x_k^{(1)} = x_k$ yield

$$\begin{aligned} & \|\tilde{x}_k^{(m)} - x_k^{(m)}\| \tag{28} \\ & \leq L_{g,0}(L_{g,0}W_{\max,2})^{m-1} \sum_{k'=k-(M-m+1)}^{k-1} \|\Delta_{k'}^{(m-1)}\| + L_{g,0}W_{\max,2}\|\tilde{x}_k^{(m-1)} - x_k^{(m-1)}\| \\ & \leq L_{g,0} \sum_{m'=2}^m (L_{g,0}W_{\max,2})^{m'-1} (L_{g,0}W_{\max,2})^{m-m'} \sum_{k'=k-(M-m'+1)}^{k-1} \|\Delta_{k'}^{(m'-1)}\| \\ & \leq L_{g,0}(L_{g,0}W_{\max,2})^{m-1} \sum_{m'=2}^m \sum_{k'=k-(M-m'+1)}^{k-1} \|\Delta_{k'}^{(m'-1)}\|. \\ & = L_{g,0}(L_{g,0}W_{\max,2})^{m-1} \sum_{m'=1}^{m-1} \sum_{k'=k-(M-m')}^{k-1} \|\Delta_{k'}^{(m')}\|. \end{aligned}$$

where the last inequality reindexes m' in the first summation.

Noticing that (25)-(28) also implies that

$$\|z_k^{(m)} - \tilde{z}_k^{(m)}\| \leq (L_{g,0}W_{\max,2})^{m-1} \sum_{m'=1}^{m-1} \sum_{k'=k-(M-m')}^{k-1} \|\Delta_{k'}^{(m')}\|. \tag{29}$$

We then bound the delay of the backward signal $\tilde{\delta}_k^{(m)}$ for $m \in [M-1]$

$$\begin{aligned} & \|\tilde{\delta}_k^{(m)} - \delta_k^{(m)}\| = \|\delta_k^{(m+1)} W_k^{(m+1)} \nabla g^{(m)}(z_k^{(m)}) - \tilde{\delta}_k^{(m+1)} W_k^{(m+1)} \nabla g^{(m)}(\tilde{z}_k^{(m)})\| \tag{30} \\ & \leq \|\delta_k^{(m+1)} - \tilde{\delta}_k^{(m+1)}\| \|W_k^{(m+1)}\| \|\nabla g^{(m)}(z_k^{(m)})\| \\ & \quad + \|\tilde{\delta}_k^{(m+1)}\| \|W_k^{(m+1)}\| \|\nabla g^{(m)}(z_k^{(m)}) - \nabla g^{(m)}(\tilde{z}_k^{(m)})\| \\ & \leq L_{g,0}W_{\max,2} \|\delta_k^{(m+1)} - \tilde{\delta}_k^{(m+1)}\| + W_{\max,2}(L_{g,0}W_{\max,2})^{M-m-1} L_{\ell,0}L_{g,0}L_{g,1} \|z_k^{(m)} - \tilde{z}_k^{(m)}\| \end{aligned}$$

where the last inequality comes from Assumption 3 (1)-(2) and Lemma 3. Substituting (29) into (30), we can further bound (30) by

$$\begin{aligned} & \|\tilde{\delta}_k^{(m)} - \delta_k^{(m)}\| \tag{31} \\ & \leq L_{g,0}W_{\max,2} \|\delta_k^{(m+1)} - \tilde{\delta}_k^{(m+1)}\| \\ & \quad + W_{\max,2}(L_{g,0}W_{\max,2})^{M-m-1} L_{\ell,0}L_{g,0}L_{g,1} (L_{g,0}W_{\max,2})^{m-1} \sum_{m'=1}^{m-1} \sum_{k'=k-(M-m'+1)}^{k-1} \|\Delta_{k'}^{(m')}\| \\ & = L_{g,0}W_{\max,2} \|\delta_k^{(m+1)} - \tilde{\delta}_k^{(m+1)}\| \\ & \quad + (L_{g,0}W_{\max,2})^{M-1} L_{\ell,0}L_{g,1} \sum_{m'=1}^{m-1} \sum_{k'=k-(M-m'+1)}^{k-1} \|\Delta_{k'}^{(m')}\| \\ & \leq (L_{g,0}W_{\max,2})^{M-m} \|\delta_k^{(M)} - \tilde{\delta}_k^{(M)}\| + (L_{g,0}W_{\max,2})^{M-1} L_{\ell,0}L_{g,1} \times \\ & \quad \sum_{m''=m}^{M-1} (L_{g,0}W_{\max,2})^{M-1-m''} \sum_{m'=1}^{m''-1} \sum_{k'=k-(M-m'+1)}^{k-1} \|\Delta_{k'}^{(m')}\|. \end{aligned}$$

To bound the first term in the RHS of (31), we manipulate the different $\|\delta_k^{(M)} - \tilde{\delta}_k^{(M)}\|$ by

$$\|\delta_k^{(M)} - \tilde{\delta}_k^{(M)}\| \tag{32}$$

$$\begin{aligned}
&= \|\nabla_{x^{(M+1)}} \ell(x_k^{(M+1)}, y_k) \nabla g^{(M)}(z_k^{(M)}) - \nabla_{x^{(M+1)}} \ell(\tilde{x}_k^{(M+1)}, y_k) \nabla g^{(M)}(\tilde{z}_k^{(M)})\| \\
&\leq \|\nabla_{x^{(M+1)}} \ell(x_k^{(M+1)}, y_k) - \nabla_{x^{(M+1)}} \ell(\tilde{x}_k^{(M+1)}, y_k)\| \|\nabla g^{(M)}(z_k^{(M)})\| \\
&\quad + \|\nabla_{x^{(M+1)}} \ell(\tilde{x}_k^{(M+1)}, y_k)\| \|\nabla g^{(M)}(\tilde{z}_k^{(M)}) - \nabla g^{(M)}(z_k^{(M)})\| \\
&\stackrel{(a)}{\leq} L_{\ell,1} L_{g,0} \|x_k^{(M+1)} - \tilde{x}_k^{(M+1)}\| + L_{\ell,0} L_{g,1} \|\tilde{z}_k^{(M)} - z_k^{(M)}\| \\
&\leq (L_{\ell,1} L_{g,0}^2 + L_{\ell,0} L_{g,1}) \|\tilde{z}_k^{(M)} - z_k^{(M)}\| \\
&\leq (L_{\ell,1} L_{g,0}^2 + L_{\ell,0} L_{g,1}) (L_{g,0} W_{\max,2})^{M-1} \sum_{m'=1}^M \sum_{k'=k-(M-m'+1)}^{k-1} \|\Delta_{k'}^{(m')}\|.
\end{aligned}$$

where (a) comes from Assumption 3 and Assumption 4.

To bound the second term in the RHS of (31), we change the upper bound of the second summation from m'' to M and get

$$\sum_{m''=m}^{M-1} (L_{g,0} W_{\max,2})^{M-1-m''} \sum_{m'=1}^{m''-1} \sum_{k'=k-(M-m'+1)}^{k-1} \|\Delta_{k'}^{(m')}\| \quad (33)$$

$$\leq \sum_{m''=m}^{M-1} (L_{g,0} W_{\max,2})^{M-1-m''} \sum_{m'=1}^M \sum_{k'=k-(M-m'+1)}^{k-1} \|\Delta_{k'}^{(m')}\| \quad (34)$$

$$= \frac{1 - (L_{g,0} W_{\max,2})^{M-m}}{1 - L_{g,0} W_{\max,2}} \sum_{m'=1}^M \sum_{k'=k-(M-m'+1)}^{k-1} \|\Delta_{k'}^{(m')}\|. \quad (35)$$

Substituting (32) and (33) back into (31) we have

$$\|\tilde{\delta}_k^{(m)} - \delta_k^{(m)}\| \leq C_\delta^{(m)} \sum_{m'=1}^M \sum_{k'=k-(M-m'+1)}^{k-1} \|\Delta_{k'}^{(m')}\| \quad (36)$$

where the constant $C_\delta^{(m)}$ is defined by

$$\begin{aligned}
C_\delta^{(m)} &:= (L_{g,0} W_{\max,2})^{M-m+1} (L_{\ell,1} L_{g,0}^2 + L_{\ell,0} L_{g,1}) (L_{g,0} W_{\max,2})^{M-1} \\
&\quad + (L_{g,0} W_{\max,2})^{M-1} L_{\ell,0} L_{g,1} \frac{1 - (L_{g,0} W_{\max,2})^{M-m}}{1 - L_{g,0} W_{\max,2}}.
\end{aligned} \quad (37)$$

This completes the proof. \square

Lemma 5 (delay error of gradient). *Suppose Assumption 2–4 hold. Denote the stale gradient by*

$$\tilde{\nabla}_{W^{(m)}}^k f := \tilde{\delta}_k^{(m)} \otimes \tilde{x}_k^{(m)}. \quad (38)$$

The gradient delay is bounded by

$$\|\tilde{\nabla}_{W^{(m)}}^k f - \nabla_{W^{(m)}} f(W_k; \xi_k)\| = C_f^{(m)} \sum_{m'=1}^M \sum_{k'=k-(M-m'+1)}^{k-1} \|\Delta_{k'}^{(m'-1)}\|. \quad (39)$$

where the constant $C_f^{(m)}$ is defined by

$$C_f^{(m)} := (L_{g,0} W_{\max,2})^m C_\delta^{(m)} + (L_{g,0} W_{\max,2})^{M-m} L_{\ell,0} L_{g,0} C_x^{(m)}. \quad (40)$$

Consequently, the norm square of the gradient delay is bounded by

$$\|\tilde{\nabla}^k f - \nabla f(W_k; \xi_k)\|^2 = C_f^2 \sum_{m'=1}^M \sum_{k'=k-(M-m'+1)}^{k-1} \|\Delta_{k'}^{(m')}\|^2 \quad (41)$$

where the constant C_f is defined by

$$C_f := M \sqrt{\sum_{m=1}^M (C_f^{(m)})^2}. \quad (42)$$

Proof of Lemma 5. By definition, the delay error is bounded by

$$\begin{aligned}
& \|\tilde{\nabla}_{W^{(m)}}^k f - \nabla_{W^{(m)}} f(W_k; \xi_k)\| \\
&= \|\tilde{\delta}_k^{(m)} \otimes \tilde{x}_k^{(m)} - \delta_k^{(m)} \otimes x_k^{(m)}\| \\
&= \|(\tilde{\delta}_k^{(m)} - \delta_k^{(m)}) \otimes \tilde{x}_k^{(m)} + \delta_k^{(m)} \otimes (\tilde{x}_k^{(m)} - x_k^{(m)})\| \\
&\leq \|\tilde{\delta}_k^{(m)} - \delta_k^{(m)}\| \|\tilde{x}_k^{(m)}\| + \|\delta_k^{(m)}\| \|\tilde{x}_k^{(m)} - x_k^{(m)}\|.
\end{aligned} \tag{43}$$

According to Lemma 3 and Lemma 4, it follows that

$$\begin{aligned}
& \|\tilde{\nabla}_{W^{(m)}}^k f - \nabla_{W^{(m)}} f(W_k; \xi_k)\| \\
&\leq ((L_{g,0} W_{\max,2})^m C_\delta^{(m)} + (L_{g,0} W_{\max,2})^{M-m} L_{\ell,0} L_{g,0} C_x^{(m)}) \sum_{m'=1}^M \sum_{k'=k-(M-m'+1)}^{k-1} \|\Delta_{k'}^{(m')}\|^2 \\
&= C_f^{(m)} \sum_{m'=1}^M \sum_{k'=k-(M-m'+1)}^{k-1} \|\Delta_{k'}^{(m')}\|^2.
\end{aligned} \tag{44}$$

It completes the proof. \square

C Smoothness of the object

This section proves Lemma 1, i.e. the object is L -smooth. Before that, we introduce a lemma as the step stone.

Since the definition of function smoothness involves two weights W , W' and both of them generate a sequence of forward and backward signals, we require symbols to represent them. Using slightly abusing notation in this section, we denote the forward signals computed by W and \tilde{W} as $x^{(m)}$ and $\tilde{x}^{(m)}$, respectively, and denote the backward signals as $\delta^{(m)}$ and $\tilde{\delta}^{(m)}$, respectively.

Lemma 6 (Signal stability). *Denote the forward signals computed by W and \tilde{W} as $x^{(m)}$ and $\tilde{x}^{(m)}$, respectively, and denote the backward signals as $\delta^{(m)}$ and $\tilde{\delta}^{(m)}$, respectively.*

$$\|\tilde{x}^{(m)} - x^{(m)}\|^2 \leq C_{x'}^{(m)} \|\tilde{W} - W\|^2, \tag{45}$$

$$\|\tilde{z}^{(m)} - z^{(m)}\|^2 \leq C_{z'}^{(m)} \|\tilde{W} - W\|^2, \tag{46}$$

$$\|\tilde{\delta}^{(m)} - \delta^{(m)}\|^2 \leq C_{\delta'}^{(m)} \|\tilde{W} - W\|^2, \tag{47}$$

where the constants $C_x^{(m)}$ and $C_z^{(m)}$ are defined by

$$C_{x'}^{(m)} := 2L_{g,0} (L_{g,0} W_{\max,2})^{2(m-1)}, \tag{48}$$

$$C_{z'}^{(m)} := 2(L_{g,0} W_{\max,2})^{2(m-1)}, \tag{49}$$

and $C_{\delta'}^{(m)}$ is defined by

$$\begin{aligned}
C_{\delta'}^{(m)} &:= 3(L_{g,0} W_{\max,2})^2 (2L_{\ell,1}^2 L_{g,0}^4 + 2L_{\ell,0}^2 L_{g,1}^2) (L_{g,0} W_{\max,2})^{2(M-1)} \\
&+ 3(L_{g,0} W_{\max,2})^{2(M-m)} L_{\ell,0}^2 L_{g,0}^4 \sum_{m''=m}^{M-1} (L_{g,0} W_{\max,2})^{2(M-1-m'')} \frac{1 - (L_{g,0} W_{\max,2})^{2(M-m)}}{1 - L_{g,0} W_{\max,2}} \\
&+ 3(L_{g,0} W_{\max,2})^{2(M-1)} L_{\ell,0}^2 L_{g,1}^2 \sum_{m''=m}^{M-1} (L_{g,0} W_{\max,2})^{2(M-1-m'')} \frac{1 - (L_{g,0} W_{\max,2})^{2(M-m)}}{1 - L_{g,0} W_{\max,2}}.
\end{aligned} \tag{50}$$

Proof of Lemma 6. We first bound the delay of forward signal $\tilde{x}_k^{(m)}$. At the first layer, there is no delay, i.e. $\tilde{x}^{(1)} = x^{(1)} = x$. For other layers $m \geq 1$

$$\begin{aligned}
& \|\tilde{x}^{(m+1)} - x^{(m+1)}\|^2 \leq L_{g,0}^2 \|\tilde{z}^{(m)} - z^{(m)}\|^2 & (51) \\
& = L_{g,0}^2 \|\tilde{W}^{(m)} \tilde{x}^{(m)} - W^{(m)} x^{(m)}\|^2 \\
& = L_{g,0}^2 \|(\tilde{W}^{(m)} - W^{(m)}) \tilde{x}^{(m)} + W^{(m)} (\tilde{x}^{(m)} - x^{(m)})\|^2 \\
& \leq 2L_{g,0}^2 (\|\tilde{W}^{(m)} - W^{(m)}\|^2 \|\tilde{x}^{(m)}\|^2 + \|W^{(m)}\|^2 \|\tilde{x}^{(m)} - x^{(m)}\|^2) \\
& \leq 2L_{g,0}^2 ((L_{g,0} W_{\max,2})^{2m} \|\tilde{W}^{(m)} - W^{(m)}\|^2 + W_{\max,2}^2 \|\tilde{x}^{(m)} - x^{(m)}\|^2).
\end{aligned}$$

Expanding inequality (51) from m to 1 and using the fact $\tilde{x}^{(1)} = x^{(1)} = x$ yield

$$\begin{aligned}
& \|\tilde{x}^{(m)} - x^{(m)}\|^2 & (52) \\
& \leq 2L_{g,0}^2 (L_{g,0} W_{\max,2})^{2(m-1)} \|\tilde{W}^{(m-1)} - W^{(m-1)}\|^2 + 2L_{g,0}^2 W_{\max,2}^2 \|\tilde{x}^{(m-1)} - x^{(m-1)}\|^2 \\
& \leq 2L_{g,0}^2 \sum_{m'=2}^m (L_{g,0} W_{\max,2})^{2(m'-1)} (L_{g,0} W_{\max,2})^{2(m-m')} \|\tilde{W}^{(m'-1)} - W^{(m'-1)}\|^2 \\
& = 2L_{g,0}^2 (L_{g,0} W_{\max,2})^{2(m-1)} \sum_{m'=2}^m \|\tilde{W}^{(m'-1)} - W^{(m'-1)}\|^2 \\
& = 2L_{g,0}^2 (L_{g,0} W_{\max,2})^{2(m-1)} \sum_{m'=1}^{m-1} \|\tilde{W}^{(m')} - W^{(m')}\|^2 & (53)
\end{aligned}$$

where the last equality reindexes the summation. By applying the relation

$$\sum_{m'=1}^{m-1} \|\tilde{W}^{(m')} - W^{(m')}\|^2 \leq \sum_{m'=1}^M \|\tilde{W}^{(m')} - W^{(m')}\|^2 = \|\tilde{W} - W\|^2 & (54)$$

we prove (45). Inferring in the similar way of (51)-(52), we obtain (46)

$$\|\tilde{z}^{(m)} - z^{(m)}\|^2 \leq 2(L_{g,0} W_{\max,2})^{2(m-1)} \|\tilde{W} - W\|^2 & (55)$$

We then bound the difference of the backward signal $\tilde{\delta}^{(m)}$ for $m \in [M-1]$

$$\begin{aligned}
& \|\tilde{\delta}^{(m)} - \delta^{(m)}\|^2 = \|\tilde{\delta}^{(m+1)} \tilde{W}^{(m+1)} \nabla g^{(m)}(z^{(m)}) - \delta^{(m+1)} W^{(m+1)} \nabla g^{(m)}(z^{(m)})\|^2 & (56) \\
& \leq 3\|\tilde{\delta}^{(m+1)} - \delta^{(m+1)}\|^2 \|\tilde{W}^{(m+1)}\|^2 \|\nabla g^{(m)}(z^{(m)})\|^2 \\
& \quad + 3\|\delta^{(m+1)}\|^2 \|\tilde{W}^{(m+1)} - W^{(m+1)}\|^2 \|\nabla g^{(m)}(z^{(m)})\|^2 \\
& \quad + 3\|\delta^{(m+1)}\|^2 \|W^{(m+1)}\|^2 \|\nabla g^{(m)}(z^{(m)}) - \nabla g^{(m)}(\tilde{z}^{(m)})\|^2 \\
& \leq 3(L_{g,0} W_{\max,2})^2 \|\tilde{\delta}^{(m+1)} - \delta^{(m+1)}\|^2 + 3(L_{g,0} W_{\max,2})^{2(M-m)} L_{\ell,0}^2 L_{g,0}^4 \|\tilde{W}^{(m+1)} - W^{(m+1)}\|^2 \\
& \quad + 3W_{\max,2}^2 (L_{g,0} W_{\max,2})^{2(M-m-1)} L_{\ell,0}^2 L_{g,0}^2 L_{g,1}^2 \|z^{(m)} - \tilde{z}^{(m)}\|^2
\end{aligned}$$

where the last inequality comes from Assumption 3 (1)-(2) and Lemma 3. Substituting (55) into (56), we can further bound (56) by

$$\begin{aligned}
& \|\tilde{\delta}^{(m)} - \delta^{(m)}\|^2 \tag{57} \\
& \leq 3L_{g,0}^2 W_{\max,2}^2 \|\tilde{\delta}^{(m+1)} - \delta^{(m+1)}\|^2 + 3(L_{g,0} W_{\max,2})^{2(M-m)} L_{\ell,0}^2 L_{g,0}^4 \|\tilde{W}^{(m+1)} - W^{(m+1)}\|^2 \\
& \quad + 3W_{\max,2}^2 (L_{g,0} W_{\max,2})^{2(M-m-1)} L_{\ell,0}^2 L_{g,0}^2 L_{g,1}^2 (L_{g,0} W_{\max,2})^{2(m-1)} \sum_{m'=1}^{m-1} \|\tilde{W}^{(m')} - W^{(m')}\|^2 \\
& = 3L_{g,0}^2 W_{\max,2}^2 \|\tilde{\delta}^{(m+1)} - \delta^{(m+1)}\|^2 + 3(L_{g,0} W_{\max,2})^{2(M-m)} L_{\ell,0}^2 L_{g,0}^4 \|\tilde{W}^{(m+1)} - W^{(m+1)}\|^2 \\
& \quad + 3(L_{g,0} W_{\max,2})^{2(M-1)} L_{\ell,0}^2 L_{g,1}^2 \sum_{m'=1}^{m-1} \|\tilde{W}^{(m')} - W^{(m')}\|^2 \\
& \leq 3(L_{g,0} W_{\max,2})^{2(M-m)} \|\delta^{(M)} - \tilde{\delta}^{(M)}\|^2 \\
& \quad + 3(L_{g,0} W_{\max,2})^{2(M-m)} L_{\ell,0}^2 L_{g,0}^4 \sum_{m''=m}^{M-1} (L_{g,0} W_{\max,2})^{2(M-1-m'')} \|\tilde{W}^{(m''+1)} - W^{(m''+1)}\|^2 \\
& \quad + 3(L_{g,0} W_{\max,2})^{2(M-1)} L_{\ell,0}^2 L_{g,1}^2 \sum_{m''=m}^{M-1} (L_{g,0} W_{\max,2})^{2(M-1-m'')} \sum_{m'=1}^{m''-1} \|\tilde{W}^{(m')} - W^{(m')}\|^2.
\end{aligned}$$

To bound the first term in the RHS of (57), we manipulate the different $\|\delta^{(M)} - \tilde{\delta}^{(M)}\|$ by

$$\begin{aligned}
& \|\delta^{(M)} - \tilde{\delta}^{(M)}\|^2 \tag{58} \\
& = \|\nabla_{x^{(M+1)}} \ell(x^{(M+1)}, y) \nabla g^{(M)}(z^{(M)}) - \nabla_{x^{(M+1)}} \ell(\tilde{x}^{(M+1)}, y) \nabla g^{(M)}(\tilde{z}^{(M)})\|^2 \\
& \leq 2\|\nabla_{x^{(M+1)}} \ell(x^{(M+1)}, y) - \nabla_{x^{(M+1)}} \ell(\tilde{x}^{(M+1)}, y)\|^2 \|\nabla g^{(M)}(z^{(M)})\|^2 \\
& \quad + 2\|\nabla_{x^{(M+1)}} \ell(\tilde{x}^{(M+1)}, y)\|^2 \|\nabla g^{(M)}(\tilde{z}^{(M)}) - \nabla g^{(M)}(z^{(M)})\|^2 \\
& \stackrel{(a)}{\leq} 2L_{\ell,1}^2 L_{g,0}^2 \|x^{(M+1)} - \tilde{x}^{(M+1)}\|^2 + 2L_{\ell,0}^2 L_{g,1}^2 \|\tilde{z}^{(M)} - z^{(M)}\|^2 \\
& \leq (2L_{\ell,1}^2 L_{g,0}^4 + 2L_{\ell,0}^2 L_{g,1}^2) \|\tilde{z}^{(M)} - z^{(M)}\|^2 \\
& \leq (2L_{\ell,1}^2 L_{g,0}^4 + 2L_{\ell,0}^2 L_{g,1}^2) (L_{g,0} W_{\max,2})^{2(M-1)} \sum_{m'=1}^{M-1} \|\tilde{W}^{(m')} - W^{(m')}\|^2.
\end{aligned}$$

where (a) comes from Assumption 3 and Assumption 4.

To bound the second term in the RHS of (57), we add some terms into the summation

$$\begin{aligned}
& \sum_{m''=m}^{M-1} (L_{g,0} W_{\max,2})^{2(M-1-m'')} \|\tilde{W}^{(m''+1)} - W^{(m''+1)}\|^2 \tag{59} \\
& \leq \sum_{m''=m}^{M-1} (L_{g,0} W_{\max,2})^{2(M-1-m'')} \sum_{m'=1}^M \|\tilde{W}^{(m')} - W^{(m')}\|^2 \\
& = \frac{1 - (L_{g,0} W_{\max,2})^{2(M-m)}}{1 - L_{g,0} W_{\max,2}} \sum_{m'=1}^M \|\tilde{W}^{(m')} - W^{(m')}\|^2.
\end{aligned}$$

To bound the third term in the RHS of (57), we change the upper bound of the second summation from m'' to M and get

$$\begin{aligned}
& \sum_{m''=m}^{M-1} (L_{g,0}W_{\max,2})^{2(M-1-m'')} \sum_{m'=1}^{m''-1} \|\tilde{W}^{(m')} - W^{(m')}\|^2 \quad (60) \\
& \leq \sum_{m''=m}^{M-1} (L_{g,0}W_{\max,2})^{2(M-1-m'')} \sum_{m'=1}^M \|\tilde{W}^{(m')} - W^{(m')}\|^2 \\
& = \frac{1 - (L_{g,0}W_{\max,2})^{2(M-m)}}{1 - L_{g,0}W_{\max,2}} \sum_{m'=1}^M \|\tilde{W}^{(m')} - W^{(m')}\|^2.
\end{aligned}$$

Substituting (58)–(60) back into (57) we have

$$\|\tilde{\delta}^{(m)} - \delta^{(m)}\|^2 \leq C_{\delta'}^{(m)} \sum_{m'=1}^M \|\tilde{W}^{(m')} - W^{(m')}\|^2 \quad (61)$$

This completes the proof. \square

Lemma 7 (smoothness of the objective, restatement of Lemma 1). *Under Assumption 2–5, the objective is L -smooth with respect to W , i.e. $\forall \xi = (x, y) \in \mathcal{X} \times \mathcal{Y}$,*

$$\|\nabla f(W; \xi) - \nabla f(\tilde{W}; \xi)\| \leq L_f \|W - \tilde{W}\| \quad (62)$$

where the smoothness constant is defined as

$$L_f := \sqrt{2 \sum_{m=1}^M ((L_{g,0}W_{\max,2})^{2m} C_{\delta'}^{(m)} + (L_{g,0}W_{\max,2})^{2(M-m)} L_{\ell,0}^2 L_{g,0}^2 C_{x'}^{(m)})}. \quad (63)$$

Proof of Lemma 1 and Lemma 7. Analogous to the proof of Lemma (6), we use $x^{(m)}/\delta^{(m)}$ and $\tilde{x}^{(m)}/\tilde{\delta}^{(m)}$ to denote the forward/backward signals related to W and \tilde{W} , respectively. It follows by definition of gradient (4) that

$$\|\nabla f(W; \xi) - \nabla f(\tilde{W}; \xi)\|^2 \quad (64)$$

$$\begin{aligned}
& = \sum_{m=1}^M \|\nabla_{W^{(m)}} f(W; \xi) - \nabla_{W^{(m)}} f(\tilde{W}; \xi)\|^2 \quad (65) \\
& = \sum_{m=1}^M \|\tilde{\delta}^{(m)} \otimes \tilde{x}^{(m)} - \delta^{(m)} \otimes x^{(m)}\|^2 \\
& = \sum_{m=1}^M \|(\tilde{\delta}^{(m)} - \delta^{(m)}) \otimes \tilde{x}^{(m)} + \delta^{(m)} \otimes (\tilde{x}^{(m)} - x^{(m)})\|^2 \\
& \leq 2 \sum_{m=1}^M \|\tilde{\delta}^{(m)} - \delta^{(m)}\|^2 \|\tilde{x}^{(m)}\|^2 + 2 \|\delta^{(m)}\|^2 \|\tilde{x}^{(m)} - x^{(m)}\|^2.
\end{aligned}$$

According to Lemma 3 and Lemma 6, it follows that

$$\begin{aligned}
& \|\nabla f(W; \xi) - \nabla f(\tilde{W}; \xi)\|^2 \quad (66) \\
& \leq 2 \sum_{m=1}^M ((L_{g,0}W_{\max,2})^{2m} C_{\delta'}^{(m)} + (L_{g,0}W_{\max,2})^{2(M-m)} L_{\ell,0}^2 L_{g,0}^2 C_{x'}^{(m)}) \|\tilde{W} - W\|^2 \\
& = L_f^2 \|\tilde{W} - W\|^2.
\end{aligned}$$

Taking square root on both sides on (66) completes the proof. \square

D Proof of Theorem 1: Analog SGD with synchronous pipeline

This section provides the convergence guarantee of the Analog SGD with synchronous pipeline, whose iteration is

$$W_{k,b+1}^{(m)} = W_{k,b}^{(m)} - \frac{\alpha}{B} \nabla_{W^{(m)}} f(W_k; \xi_{k,b}) - \frac{\alpha}{\tau B} |\nabla_{W^{(m)}} f(W_k; \xi_{k,b})| \odot W_{k,b}^{(m)}. \quad (67)$$

Theorem 1 (Convergence rate, synchronous pipeline). *Under Assumption 1–5, if the learning rate is set as $\alpha = \sqrt{\frac{B(f(W_0) - f^*)}{\sigma^2 L_f K}}$ and K is sufficiently large such that $\alpha \leq \frac{1}{L}$, it holds that*

$$\frac{1}{K} \sum_{k=0}^{K-1} \mathbb{E}[\|\nabla f(W_k)\|^2] \leq 4\sqrt{\frac{(f(W_0) - f^*)\sigma^2 L_f}{BK}} \frac{1}{1 - W_{\max}^2/\tau^2} + \sigma^2 S$$

where S denotes the amplification factor given by $S := \frac{W_{\max}/\tau^2}{1 - W_{\max}^2/\tau^2}$.

Proof of Theorem 1. Denote the average gradient by

$$\bar{\nabla} f(W_k; \xi_k) := \frac{1}{B} \sum_{b=1}^B \nabla f(W_k; \xi_{k,b}), \quad (68)$$

which satisfies that $\mathbb{E}_{\{\xi_{k,b}: b \in [B]\}}[\bar{\nabla} f(W_k; \xi_k)] = \nabla f(W_k)$. Furthermore, the independence of sampling (c.f. Assumption 1) ensures that

$$\begin{aligned} & \mathbb{E}_{\{\xi_{k,b}: b \in [B]\}}[\|\bar{\nabla} f(W_k; \xi_k) - \nabla f(W_k)\|^2] \\ &= \mathbb{E}_{\{\xi_{k,b}: b \in [B]\}}[\|\frac{1}{B} \sum_{b=1}^B \nabla f(W_k; \xi_{k,b}) - \nabla f(W_k)\|^2] \\ &= \frac{1}{B^2} \sum_{b=1}^B \mathbb{E}_{\xi_{k,b}}[\|\nabla f(W_k; \xi_{k,b}) - \nabla f(W_k)\|^2] \\ &\leq \sigma^2/B. \end{aligned} \quad (69)$$

The L -smooth assumption of the objective (c.f. Lemma 7) implies that

$$\begin{aligned} & \mathbb{E}_{\{\xi_{k,b}: b \in [B]\}}[f(W_{k+1})] \\ &\leq f(W_k) + \mathbb{E}_{\{\xi_{k,b}: b \in [B]\}}[\langle \nabla f(W_k), W_{k+1} - W_k \rangle] + \frac{L_f}{2} \mathbb{E}_{\{\xi_{k,b}: b \in [B]\}}[\|W_{k+1} - W_k\|^2] \\ &\leq f(W_k) - \frac{\alpha}{2} \|\nabla f(W_k)\|^2 - (\frac{1}{2\alpha} - L_f) \mathbb{E}_{\varepsilon_k}[\|W_{k+1} - W_k + \alpha(\bar{\nabla} f(W_k; \xi_k) - \nabla f(W_k))\|^2] \\ &\quad + \alpha^2 L_f \mathbb{E}_{\varepsilon_k}[\|\bar{\nabla} f(W_k; \xi_k) - \nabla f(W_k)\|^2] + \frac{1}{2\alpha} \|W_{k+1} - W_k + \alpha(\nabla f(W_k) + \varepsilon_k)\|^2 \end{aligned} \quad (70)$$

where the second inequality comes from the assumption that noise has expectation 0 (Assumption 1)

$$\begin{aligned} & \mathbb{E}_{\varepsilon_k}[\langle \nabla f(W_k), W_{k+1} - W_k \rangle] \\ &= \mathbb{E}_{\varepsilon_k}[\langle \nabla f(W_k), W_{k+1} - W_k + \alpha(\bar{\nabla} f(W_k; \xi_k) - \nabla f(W_k)) \rangle] \\ &= -\frac{\alpha}{2} \|\nabla f(W_k)\|^2 - \frac{1}{2\alpha} \mathbb{E}_{\varepsilon_k}[\|W_{k+1} - W_k + \alpha(\bar{\nabla} f(W_k; \xi_k) - \nabla f(W_k))\|^2] \\ &\quad + \frac{1}{2\alpha} \mathbb{E}_{\varepsilon_k}[\|W_{k+1} - W_k + \alpha \bar{\nabla} f(W_k; \xi_k)\|^2] \end{aligned} \quad (71)$$

and the following inequality

$$\begin{aligned} & \frac{L_f}{2} \mathbb{E}_{\varepsilon_k}[\|W_{k+1} - W_k\|^2] \\ &\leq L_f \mathbb{E}_{\{\xi_{k,b}: b \in [B]\}}[\|W_{k+1} - W_k + \alpha(\bar{\nabla} f(W_k; \xi_k) - \nabla f(W_k))\|^2] \\ &\quad + \alpha^2 L \mathbb{E}_{\{\xi_{k,b}: b \in [B]\}}[\|\bar{\nabla} f(W_k; \xi_k) - \nabla f(W_k)\|^2]. \end{aligned} \quad (72)$$

With the learning rate $\alpha \leq \frac{1}{2L}$ and bounded variance (c.f. (69)), (70) becomes

$$\begin{aligned} & \mathbb{E}_{\{\xi_{k,b}: b \in [B]\}} [f(W_{k+1})] \\ & \leq f(W_k) - \frac{\alpha}{2} \|\nabla f(W_k)\|^2 + \frac{\alpha^2 L_f \sigma^2}{B} + \frac{1}{2\alpha} \mathbb{E}_{\{\xi_{k,b}: b \in [B]\}} [\|W_{k+1} - W_k + \alpha \bar{\nabla} f(W_k; \xi_k)\|^2]. \end{aligned} \quad (73)$$

According the dynamic of Analog SGD (5), the last term in the RHS of (73) is upper bounded by

$$\begin{aligned} & \frac{1}{2\alpha} \mathbb{E}_{\{\xi_{k,b}: b \in [B]\}} [\|W_{k+1} - W_k + \alpha \bar{\nabla} f(W_k; \xi_k)\|^2] \\ & = \frac{\alpha}{2\tau^2} \mathbb{E}_{\{\xi_{k,b}: b \in [B]\}} \left[\left\| \frac{1}{B} \sum_{b=1}^B |\nabla f(W_k; \xi_{k,b})| \odot W_{k,b} \right\|^2 \right] \\ & \leq \frac{\alpha}{2\tau^2} \frac{1}{B} \sum_{b=1}^B \mathbb{E}_{\xi_{k,b}} [\| |\nabla f(W_k; \xi_{k,b})| \odot W_{k,b} \|^2] \\ & \leq \frac{\alpha}{2\tau^2} \max_{b \in [B]} \|W_{k,b}\|_\infty^2 \frac{1}{B} \sum_{b=1}^B \mathbb{E}_{\xi_{k,b}} [\|\nabla f(W_k; \xi_{k,b})\|^2]. \end{aligned} \quad (74)$$

By the variance decomposition and Assumption 1, the term above can be bounded by

$$\begin{aligned} \mathbb{E}_{\xi_{k,b}} [\|f(W_k; \xi_{k,b})\|^2] & = \|\nabla f(W_k)\|^2 + \mathbb{E}_{\xi_{k,b}} [\|f(W_k; \xi_{k,b}) - \nabla f(W_k)\|^2] \\ & \leq \|\nabla f(W_k)\|^2 + \sigma^2. \end{aligned} \quad (75)$$

Consequently, combining (73), (74) and (75) yields

$$\begin{aligned} & \mathbb{E}_{\{\xi_{k,b}: b \in [B]\}} [f(W_{k+1})] \\ & \leq f(W_k) - \frac{\alpha}{2} \left(1 - \frac{\max_{b \in [B]} \|W_{k,b}\|_\infty^2}{\tau^2} \right) \|\nabla f(W_k)\|^2 + \frac{\alpha^2 L_f \sigma^2}{B} + \frac{\alpha \sigma^2}{2\tau^2} \max_{b \in [B]} \|W_{k,b}\|_\infty^2. \end{aligned} \quad (76)$$

Organizing the terms, taking expectation, averaging (76) over k from 0 to $K-1$, we obtain

$$\begin{aligned} \frac{1}{K} \sum_{k=0}^{K-1} \mathbb{E} [\|\nabla f(W_k)\|^2] & \leq \frac{2(f(W_0) - \mathbb{E}[f(W_{k+1})])}{1 - W_{\max, \infty}^2 / \tau^2} + \frac{\alpha L_f \sigma^2}{B(1 - W_{\max, \infty}^2 / \tau^2)} \\ & \quad + \frac{\sigma^2}{K} \sum_{k=0}^{K-1} \frac{\max_{b \in [B]} \|W_{k,b}\|_\infty^2 / \tau^2}{1 - \max_{b \in [B]} \|W_{k,b}\|_\infty^2 / \tau^2}. \\ & \leq 4 \sqrt{\frac{(f(W_0) - f^*) \sigma^2 L_f}{BK}} \frac{1}{1 - W_{\max}^2 / \tau^2} + \sigma^2 S_K \end{aligned} \quad (77)$$

where the second inequality uses $f(W_{k+1}) \geq f^*$ and specifies $\alpha = \sqrt{\frac{B(f(W_0) - f^*)}{\sigma^2 L_f K}}$. Now we complete the proof. \square

E Proof of Theorem 2: Analog SGD with asynchronous pipeline

This section provides the convergence guarantee of the Analog SGD under non-convex assumption on asymmetric linear devices.

Theorem 2 (Convergence rate, asynchronous pipeline). *Under Assumption 1–5, if the learning rate is set as $\alpha = \sqrt{\frac{f(W_0) - f^*}{\sigma^2 L_f K}}$ and K is sufficiently large such that $\alpha \leq \frac{1}{L_f}$, it holds that*

$$\frac{1}{K} \sum_{k=0}^{K-1} \mathbb{E} [\|\nabla f(W_k)\|^2] \leq 4 \sqrt{\frac{(f(W_0) - f^*) \sigma^2 L_f}{K}} \frac{1}{1 - (1+u)W_{\max}^2 / \tau^2} + \sigma^2 S' + O\left(\frac{1+1/u}{K}\right)$$

where $u > 0$ is any number and S' denotes the amplification factor given by $S' := \frac{(1+u)W_{\max}^2 / \tau^2}{1 - (1+u)W_{\max}^2 / \tau^2}$.

Proof of Theorem 2. The L -smooth assumption of the objective (c.f. Lemma 7) implies that

$$\begin{aligned}
& \mathbb{E}_{\xi_k}[f(W_{k+1})] \\
& \leq f(W_k) + \mathbb{E}_{\xi_k}[\langle \nabla f(W_k), W_{k+1} - W_k \rangle] + \frac{L_f}{2} \mathbb{E}_{\xi_k}[\|W_{k+1} - W_k\|^2] \\
& \leq f(W_k) - \frac{\alpha}{2} \|\nabla f(W_k)\|^2 - \left(\frac{1}{2\alpha} - L_f\right) \mathbb{E}_{\xi_k}[\|W_{k+1} - W_k + \alpha(\nabla f(W_k; \xi_k) - \nabla f(W_k))\|^2] \\
& \quad + \alpha^2 L_f \mathbb{E}_{\xi_k}[\|\nabla f(W_k; \xi_k) - \nabla f(W_k)\|^2] + \frac{1}{2\alpha} \mathbb{E}_{\xi_k}[\|W_{k+1} - W_k + \alpha \nabla f(W_k; \xi_k)\|^2]
\end{aligned} \tag{78}$$

where the second inequality comes from the assumption that noise has expectation 0 (Assumption 1)

$$\begin{aligned}
& \mathbb{E}_{\xi_k}[\langle \nabla f(W_k), W_{k+1} - W_k \rangle] \\
& = \mathbb{E}_{\xi_k}[\langle \nabla f(W_k), W_{k+1} - W_k + \alpha(\nabla f(W_k; \xi_k) - \nabla f(W_k)) \rangle] \\
& = -\frac{\alpha}{2} \|\nabla f(W_k)\|^2 - \frac{1}{2\alpha} \mathbb{E}_{\xi_k}[\|W_{k+1} - W_k + \alpha(\nabla f(W_k; \xi_k) - \nabla f(W_k))\|^2] \\
& \quad + \frac{1}{2\alpha} \mathbb{E}_{\xi_k}[\|W_{k+1} - W_k + \alpha \nabla f(W_k; \xi_k)\|^2]
\end{aligned} \tag{79}$$

and the following inequality

$$\begin{aligned}
\frac{L_f}{2} \mathbb{E}_{\xi_k}[\|W_{k+1} - W_k\|^2] & \leq L_f \mathbb{E}_{\xi_k}[\|W_{k+1} - W_k + \alpha(\nabla f(W_k; \xi_k) - \nabla f(W_k))\|^2] \\
& \quad + \alpha^2 L_f \mathbb{E}_{\xi_k}[\|\nabla f(W_k; \xi_k) - \nabla f(W_k)\|^2].
\end{aligned} \tag{80}$$

With the learning rate $\alpha \leq \frac{1}{4L_f}$ and bounded variance of noise (Assumption 1), (78) becomes

$$\begin{aligned}
\mathbb{E}_{\xi_k}[f(W_{k+1})] & \leq f(W_k) - \frac{\alpha}{2} \|\nabla f(W_k)\|^2 + \alpha^2 L_f \sigma^2 + \frac{1}{2\alpha} \mathbb{E}_{\xi_k}[\|W_{k+1} - W_k + \alpha \nabla f(W_k; \xi_k)\|^2] \\
& \quad - \frac{1}{4\alpha} \mathbb{E}_{\xi_k}[\|W_{k+1} - W_k + \alpha(\nabla f(W_k; \xi_k) - \nabla f(W_k))\|^2].
\end{aligned} \tag{81}$$

By the dynamic of Analog SGD, the last in the RHS of (81) is bounded by

$$\begin{aligned}
& \frac{1}{2\alpha} \mathbb{E}_{\xi_k}[\|W_{k+1} - W_k + \alpha \nabla f(W_k; \xi_k)\|^2] \\
& = \frac{\alpha}{2} \mathbb{E}_{\xi_k}[\|\tilde{\nabla}^k f - \nabla f(W_k; \xi_k) + \frac{1}{\tau} |\tilde{\nabla}^k f| \odot W_k\|^2] \\
& = \frac{\alpha}{2} \mathbb{E}_{\xi_k}[\|\tilde{\nabla}^k f - \nabla f(W_k; \xi_k) + \frac{1}{\tau} \tilde{\nabla}^k f \odot \text{sign}(\tilde{\nabla}^k f) \odot W_k\|^2] \\
& = \frac{\alpha}{2} \mathbb{E}_{\xi_k}[\|\tilde{\nabla}^k f - \nabla f(W_k; \xi_k) + \frac{1}{\tau} (\tilde{\nabla}^k f - \nabla f(W_k; \xi_k)) \odot \text{sign}(\tilde{\nabla}^k f) \odot W_k \\
& \quad + \frac{1}{\tau} \nabla f(W_k; \xi_k) \odot \text{sign}(\tilde{\nabla}^k f) \odot W_k\|^2] \\
& = \frac{\alpha}{2} \mathbb{E}_{\xi_k}[\|(\mathbf{1} + \frac{1}{\tau} \odot \text{sign}(\tilde{\nabla}^k f) \odot W_k)(\tilde{\nabla}^k f - \nabla f(W_k; \xi_k)) \\
& \quad + \frac{1}{\tau} \nabla f(W_k; \xi_k) \odot \text{sign}(\tilde{\nabla}^k f) \odot W_k\|^2]
\end{aligned} \tag{82}$$

where $\mathbf{1}$ is the all-one vector. Using inequality $\|x + y\|^2 \leq (1 + \frac{1}{u})\|x\|^2 + (1 + u)\|y\|^2$ we obtain

$$\begin{aligned}
& \frac{1}{2\alpha} \mathbb{E}_{\xi_k}[\|W_{k+1} - W_k + \alpha \nabla f(W_k; \xi_k)\|^2] \\
& \leq \frac{\alpha}{2} (1 + \frac{1}{u}) \mathbb{E}_{\xi_k}[\|(\mathbf{1} + \frac{1}{\tau} \odot \text{sign}(\tilde{\nabla}^k f) \odot W_k) \odot (\tilde{\nabla}^k f - \nabla f(W_k; \xi_k))\|^2] \\
& \quad + \frac{\alpha}{2\tau^2} (1 + u) \mathbb{E}_{\xi_k}[\|\nabla f(W_k; \xi_k) \odot \text{sign}(\tilde{\nabla}^k f) \odot W_k\|^2]
\end{aligned} \tag{83}$$

The first term in the RHS of (83) is bounded by

$$\frac{\alpha}{2} (1 + \frac{1}{u}) \mathbb{E}_{\xi_k}[\|(\mathbf{1} + \frac{1}{\tau} \odot \text{sign}(\tilde{\nabla}^k f) \odot W_k) \odot (\tilde{\nabla}^k f - \nabla f(W_k; \xi_k))\|^2] \tag{84}$$

$$\begin{aligned}
&\leq \frac{\alpha}{2} \left(1 + \frac{1}{u}\right) \mathbb{E}_{\xi_k} [\|\mathbf{1} + \frac{1}{\tau} \odot \text{sign}(\tilde{\nabla}^k f) \odot W_k\|_\infty^2 \|\tilde{\nabla}^k f - \nabla f(W_k; \xi_k)\|^2] \\
&\leq \frac{\alpha}{2} \left(1 + \frac{1}{u}\right) (1 + W_{\max}/\tau)^2 \mathbb{E}_{\xi_k} [\|\tilde{\nabla}^k f - \nabla f(W_k; \xi_k)\|^2] \\
&\leq \frac{\alpha}{2} \left(1 + \frac{1}{u}\right) (1 + W_{\max}/\tau)^2 M^2 C_f^2 \sum_{m'=1}^M \sum_{k'=k-(M-m'+1)}^{k-1} \mathbb{E}_{\xi_k} [\|\Delta_{k'}^{(m')}\|^2].
\end{aligned}$$

where the last inequality comes from Lemma 5.

The second term in the RHS of (83) is bounded by

$$\begin{aligned}
&\frac{\alpha}{2\tau^2} (1 + u) \mathbb{E}_{\xi_k} [\|\nabla f(W_k; \xi_k) \odot \text{sign}(\tilde{\nabla}^k f) \odot W_k\|^2] \tag{85} \\
&\leq \frac{\alpha}{2\tau^2} (1 + u) \mathbb{E}_{\xi_k} [\|\nabla f(W_k; \xi_k)\|^2] \|W_k\|_\infty^2 \\
&\leq \frac{\alpha}{2\tau^2} (1 + u) \|\nabla f(W_k)\|^2 \|W_k\|_\infty^2 + \frac{\alpha\sigma^2}{2\tau^2} (1 + u) \|W_k\|_\infty^2
\end{aligned}$$

where the last inequality comes from Assumption 1

$$\begin{aligned}
\mathbb{E}_{\xi_k} [\|f(W_k; \xi_k)\|^2] &= \|\nabla f(W_k)\|^2 + \mathbb{E}_{\xi_k} [\|f(W_k; \xi_k) - \nabla f(W_k)\|^2] \tag{86} \\
&\leq \|\nabla f(W_k)\|^2 + \sigma^2.
\end{aligned}$$

Plugging (83), (84) and (85) back into (82), we have

$$\begin{aligned}
&\frac{1}{2\alpha} \mathbb{E}_{\xi_k} [\|W_{k+1} - W_k + \alpha \nabla f(W_k; \xi_k)\|^2] \tag{87} \\
&= \frac{\alpha}{2} \left(1 + \frac{1}{u}\right) (1 + W_{\max}/\tau)^2 C_f^2 M^2 \sum_{m'=1}^M \sum_{k'=k-(M-m'+1)}^{k-1} \mathbb{E}_{\xi_k} [\|\Delta_{k'}^{(m')}\|^2] \\
&\quad + \frac{\alpha}{2\tau^2} (1 + u) \|\nabla f(W_k)\|^2 \|W_k\|_\infty^2 + \frac{\alpha\sigma^2}{2\tau^2} (1 + u) \|W_k\|_\infty^2.
\end{aligned}$$

Substituting (87) into (81) yields

$$\begin{aligned}
&\mathbb{E}_{\xi_k} [f(W_{k+1})] \tag{88} \\
&\leq f(W_k) - \frac{\alpha}{2} \|\nabla f(W_k)\|^2 + \alpha^2 L_f \sigma^2 + \frac{\alpha}{2\tau^2} (1 + u) \|\nabla f(W_k)\|^2 \|W_k\|_\infty^2 + \frac{\alpha\sigma^2}{2\tau^2} (1 + u) \|W_k\|_\infty^2 \\
&\quad - \frac{1}{4\alpha} \mathbb{E}_{\xi_k} [\|W_{k+1} - W_k + \alpha(\nabla f(W_k; \xi_k) - \nabla f(W_k))\|^2] \\
&\quad + \frac{\alpha}{2} \left(1 + \frac{1}{u}\right) (1 + W_{\max}/\tau)^2 C_f^2 M^2 \sum_{m'=1}^M \sum_{k'=k-(M-m'+1)}^{k-1} \mathbb{E}_{\xi_k} [\|\Delta_{k'}^{(m')}\|^2]. \\
&= f(W_k) - \frac{\alpha}{2} \left(1 - (1 + u) \frac{\|W_k\|_\infty^2}{\tau^2}\right) \|\nabla f(W_k)\|^2 + \alpha^2 L_f \sigma^2 + \frac{\alpha\sigma^2}{2\tau^2} (1 + u) \|W_k\|_\infty^2 \\
&\quad - \frac{1}{4\alpha} \mathbb{E}_{\xi_k} [\|W_{k+1} - W_k + \alpha(\nabla f(W_k; \xi_k) - \nabla f(W_k))\|^2] \\
&\quad + \frac{\alpha}{2} \left(1 + \frac{1}{u}\right) (1 + W_{\max}/\tau)^2 C_f^2 M^2 \sum_{m'=1}^M \sum_{k'=k-(M-m'+1)}^{k-1} \mathbb{E}_{\xi_k} [\|\Delta_{k'}^{(m')}\|^2].
\end{aligned}$$

Construct a Lyapunov function by

$$\begin{aligned}
\mathbb{V}_k &:= f(W_k) - f^* \tag{89} \\
&\quad + \frac{\alpha}{2} \left(1 + \frac{1}{u}\right) (1 + W_{\max}/\tau)^2 C_f^2 M^2 \sum_{m'=1}^M \sum_{k'=k-(M-m'+1)}^{k-1} (k' - k + M + 1) \|\Delta_{k'}^{(m')}\|^2.
\end{aligned}$$

Notice that the last term above has the following recursion from k to $k + 1$

$$\sum_{m'=1}^M \sum_{k'=k+1-(M-m'+1)}^k (k' - (k + 1) + M + 1) \|\Delta_{k'}^{(m')}\|^2 \tag{90}$$

$$\begin{aligned}
&= \sum_{m'=1}^M \sum_{k'=k+1-(M-m'+1)}^k (k' - k + M + 1) \|\Delta_{k'}^{(m')}\|^2 - \sum_{m'=1}^M \sum_{k'=k+1-(M-m'+1)}^k \|\Delta_{k'}^{(m')}\|^2 \\
&= \sum_{m'=1}^M \sum_{k'=k-(M-m'+1)}^{k-1} (k' - k + M + 1) \|\Delta_{k'}^{(m')}\|^2 - \sum_{m'=1}^M \sum_{k'=k+1-(M-m'+1)}^k \|\Delta_{k'}^{(m')}\|^2 \\
&\quad + (M - m + 1) \sum_{m'=1}^M \|\Delta_{k'}^{(m')}\|^2.
\end{aligned}$$

According to (88), we have

$$\begin{aligned}
&\mathbb{E}_{\xi_k} [\mathbb{V}_{k+1}] \tag{91} \\
&= f(W_{k+1}) - f^* + \frac{\alpha C_f M^2}{2} \sum_{m'=1}^M \sum_{k'=k+1-(M-m'+1)}^k (k' - k + 1 + M + 1) \mathbb{E}_{\xi_k} [\|\Delta_{k'}^{(m'-1)}\|^2] \\
&\leq f(W_k) - \frac{\alpha}{2} \left(1 - (1+u) \frac{\|W_k\|_\infty^2}{\tau^2} \right) \|\nabla f(W_k)\|^2 + \alpha^2 L_f \sigma^2 + \frac{\alpha \sigma^2}{2\tau^2} (1+u) \|W_k\|_\infty^2 \\
&\quad - \frac{1}{4\alpha} \mathbb{E}_{\xi_k} [\|W_{k+1} - W_k + \alpha(\nabla f(W_k; \xi_k) - \nabla f(W_k))\|^2] \\
&\quad - \frac{\alpha}{2} \left(1 + \frac{1}{u} \right) (1 + W_{\max}/\tau)^2 C_f^2 M^2 \sum_{m'=1}^M \sum_{k'=k-(M-m'+1)}^k \mathbb{E}_{\xi_k} [\|\Delta_{k'}^{(m')}\|^2] \\
&\quad + \frac{\alpha}{2} \left(1 + \frac{1}{u} \right) (1 + W_{\max}/\tau)^2 C_f^2 M^3 \sum_{m'=1}^M \mathbb{E}_{\xi_k} [\|\Delta_{k'}^{(m')}\|^2].
\end{aligned}$$

By the definition of $\Delta_k^{(m)}$ and the dynamic of Analog SGD, we bound the last term of the RHS of (91) by

$$\begin{aligned}
&\sum_{m'=1}^M \|\Delta_{k'}^{(m')}\|^2 = \sum_{m'=1}^M \|W_{k+1}^{(m')} - W_k^{(m')}\|^2 = \|W_{k+1} - W_k\|^2 \tag{92} \\
&\leq 2\|W_{k+1} - W_k + \alpha(\nabla f(W_k; \xi_k) - \nabla f(W_k))\|^2 + 2\alpha^2 \|\nabla f(W_k; \xi_k) - \nabla f(W_k)\|^2 \\
&\leq 2\|W_{k+1} - W_k + \alpha(\nabla f(W_k; \xi_k) - \nabla f(W_k))\|^2 + 2\alpha^2 \sigma^2.
\end{aligned}$$

Organizing the terms of (91), we obtain

$$\begin{aligned}
&\frac{\alpha}{2} \left(1 - (1+u) \frac{\|W_k\|_\infty^2}{\tau^2} \right) \|\nabla f(W_k)\|^2 \tag{93} \\
&\leq \mathbb{V}_k - \mathbb{E}_{\xi_k} [\mathbb{V}_{k+1}] + \alpha^2 L_f \sigma^2 + \frac{\alpha \sigma^2}{2\tau^2} (1+u) \|W_k\|_\infty^2 \\
&\quad - \left(\frac{1}{4\alpha} - \alpha \left(1 + \frac{1}{u} \right) (1 + W_{\max}/\tau)^2 C_f^2 M^2 \right) \mathbb{E}_{\xi_k} [\|W_{k+1} - W_k + \alpha(\nabla f(W_k; \xi_k) - \nabla f(W_k))\|^2] \\
&\quad + \alpha^3 \left(1 + \frac{1}{u} \right) (1 + W_{\max}/\tau)^2 C_f^2 M^3 \sigma^2.
\end{aligned}$$

Taking expectation, averaging (93) over k from 0 to $K - 1$, and choosing the learning rate $\alpha \leq \frac{1}{2\sqrt{1+1/u}(1+W_{\max}/\tau)C_f M}$ yield

$$\begin{aligned}
&\frac{1}{K} \sum_{k=0}^{K-1} \mathbb{E} [\|\nabla f(W_k)\|^2] \tag{94} \\
&\leq \frac{2(\mathbb{V}_0 - \mathbb{E}[\mathbb{V}_{k+1}])}{\alpha K (1 - (1+u)W_{\max}^2/\tau^2)} + \frac{2\alpha L_f \sigma^2}{1 - (1+u)W_{\max}^2/\tau^2} \\
&\quad + \sigma^2 \frac{1}{K} \sum_{k=0}^{K-1} \frac{(1+u)\|W_k\|_\infty^2/\tau}{1 - (1+u)\|W_k\|_\infty^2/\tau^2} + \frac{\alpha^2 (1+1/u)(1+W_{\max}/\tau)^4 C_f^2 M^3 \sigma^2}{(1 - (1+u)W_{\max}^2/\tau^2)}.
\end{aligned}$$

Using the fact that $V_k \geq 0$ for any $k \in \mathbb{N}$ and $V_0 = f(W_0) - f^*$, and choosing the learning rate $\alpha = \sqrt{\frac{f(W_0) - f^*}{\sigma^2 L_f K}}$, we have

$$\begin{aligned} & \frac{1}{K} \sum_{k=0}^{K-1} \mathbb{E} [\|\nabla f(W_k)\|^2] \\ & \leq 4\sqrt{\frac{(f(W_0) - f^*)\sigma^2 L_f}{K}} \frac{1}{1 - (1+u)W_{\max}^2/\tau^2} + \sigma^2 S'_K + O\left(\frac{1+1/u}{K}\right). \end{aligned} \quad (95)$$

where S'_K denotes the amplification factor given by

$$S'_K := \frac{1}{K} \sum_{k=0}^{K-1} \frac{(1+u)\|W_k\|_{\infty}^2/\tau^2}{1 - (1+u)\|W_k\|_{\infty}^2/\tau^2} \leq \frac{(1+u)W_{\max}^2/\tau^2}{1 - (1+u)W_{\max}^2/\tau^2}. \quad (96)$$

□

F Convergence of digital asynchronous pipeline SGD

Theorem 3 (Convergence rate, asynchronous pipeline). *Under Assumption 1–5, if the learning rate is set as $\alpha = \sqrt{\frac{f(W_0) - f^*}{\sigma^2 L_f K}}$ and K is sufficiently large such that $\alpha \leq \sqrt{\frac{1}{4C_f M^3}}$, it holds that*

$$\frac{1}{K} \sum_{k=0}^{K-1} \mathbb{E} [\|\nabla f(W_k)\|^2] \leq 4\sqrt{\frac{(f(W_0) - f^*)L_f \sigma^2}{K}} + \frac{2C_f M^3 (f(W_0) - f^*)}{K L_f}. \quad (97)$$

Proof. The validation of inequality (78) does not rely on the any training algorithm and hence it still holds here. To bound the last term in the RHS of (78), we have

$$\begin{aligned} & \frac{1}{2\alpha} \mathbb{E}_{\xi_k} [\|W_{k+1} - W_k + \alpha \nabla f(W_k; \xi_k)\|^2] \\ & = \frac{\alpha}{2} \mathbb{E}_{\xi_k} [\|\tilde{\nabla}^k f - \nabla f(W_k; \xi_k)\|^2] \\ & \leq \frac{\alpha C_f}{2} \mathbb{E}_{\xi_k} \left[\sum_{m'=1}^M \sum_{k'=k-(M-m'+1)}^{k-1} \|\Delta_{k'}^{(m')}\|^2 \right]^2 \\ & \leq \frac{\alpha C_f M^2}{2} \sum_{m'=1}^M \sum_{k'=k-(M-m'+1)}^{k-1} \mathbb{E}_{\xi_k} [\|\Delta_{k'}^{(m')}\|^2] \end{aligned} \quad (98)$$

where the first inequality is according to Lemma 5.

According to the descent lemma in (81), we have

$$\begin{aligned} \mathbb{E}_{\xi_k} [f(W_{k+1})] & \leq f(W_k) - \frac{\alpha}{2} \|\nabla f(W_k)\|^2 + \alpha^2 L_f \sigma^2 + \frac{1}{2\alpha} \mathbb{E}_{\xi_k} [\|W_{k+1} - W_k + \alpha \nabla f(W_k; \xi_k)\|^2] \\ & \quad - \frac{1}{4\alpha} \mathbb{E}_{\xi_k} [\|W_{k+1} - W_k + \alpha(\nabla f(W_k; \xi_k) - \nabla f(W_k))\|^2] \\ & \leq f(W_k) - \frac{\alpha}{2} \|\nabla f(W_k)\|^2 + \alpha^2 L_f \sigma^2 + \frac{\alpha C_f M^2}{2} \sum_{m'=1}^M \sum_{k'=k-(M-m'+1)}^{k-1} \mathbb{E}_{\xi_k} [\|\Delta_{k'}^{(m')}\|^2] \\ & \quad - \frac{1}{4\alpha} \mathbb{E}_{\xi_k} [\|W_{k+1} - W_k + \alpha(\nabla f(W_k; \xi_k) - \nabla f(W_k))\|^2] \end{aligned} \quad (99)$$

where the second inequality is earned by plugging in (98).

Construct a Lyapunov function as

$$\mathbb{V}_k := f(W_k) + \frac{\alpha C_f M^2}{2} \sum_{m'=1}^M \sum_{k'=k-(M-m'+1)}^{k-1} (k' - k + M - m' + 2) \|\Delta_{k'}^{(m')}\|^2. \quad (100)$$

According to (99), we have

$$\begin{aligned}
& \mathbb{E}_{\xi_k}[\mathbb{V}_{k+1}] - \mathbb{V}_k \\
& \leq -\frac{\alpha}{2}\|\nabla f(W_k)\|^2 + \alpha^2 L_f \sigma^2 + \frac{\alpha C_f M^2}{2} \sum_{m'=1}^M \sum_{k'=k-(M-m'+1)}^{k-1} \mathbb{E}_{\xi_k}[\|\Delta_{k'}^{(m')}\|^2] \\
& \quad - \frac{1}{4\alpha} \mathbb{E}_{\xi_k}[\|W_{k+1} - W_k + \alpha(\nabla f(W_k; \xi_k) - \nabla f(W_k))\|^2] \\
& \quad + \frac{\alpha C_f M^2}{2} \sum_{m'=1}^M \sum_{k'=k-(M-m'+1)}^k (k' - k + M - m' + 1) \mathbb{E}_{\xi_k}[\|\Delta_{k'}^{(m')}\|^2] \\
& \quad - \frac{\alpha C_f M^2}{2} \sum_{m'=1}^M \sum_{k'=k-(M-m'+1)}^{k-1} (k' - k + M - m' + 2) \mathbb{E}_{\xi_k}[\|\Delta_{k'}^{(m')}\|^2] \\
& \leq -\frac{\alpha}{2}\|\nabla f(W_k)\|^2 + \alpha^2 L_f \sigma^2 + \frac{\alpha C_f M^2}{2} \sum_{m'=1}^M \sum_{k'=k-(M-m'+1)}^{k-1} \mathbb{E}_{\xi_k}[\|\Delta_{k'}^{(m')}\|^2] \\
& \quad - \frac{1}{4\alpha} \mathbb{E}_{\xi_k}[\|W_{k+1} - W_k + \alpha(\nabla f(W_k; \xi_k) - \nabla f(W_k))\|^2] \\
& \quad - \frac{\alpha C_f M^2}{2} \sum_{m'=1}^M \sum_{k'=k-(M-m'+1)}^{k-1} \mathbb{E}_{\xi_k}[\|\Delta_{k'}^{(m')}\|^2] + \frac{\alpha C_f M^2}{2} (M - m' + 1) \sum_{m'=1}^M \mathbb{E}_{\xi_k}[\|\Delta_k^{(m')}\|^2]. \\
& \leq -\frac{\alpha}{2}\|\nabla f(W_k)\|^2 + \alpha^2 L_f \sigma^2 + \frac{\alpha C_f M^2}{2} \sum_{m'=1}^M \sum_{k'=k-(M-m'+1)}^{k-1} \mathbb{E}_{\xi_k}[\|\Delta_{k'}^{(m')}\|^2] \\
& \quad - \frac{1}{4\alpha} \mathbb{E}_{\xi_k}[\|W_{k+1} - W_k + \alpha(\nabla f(W_k; \xi_k) - \nabla f(W_k))\|^2] \\
& \quad - \frac{\alpha C_f M^2}{2} \sum_{m'=1}^M \sum_{k'=k-(M-m'+1)}^{k-1} \mathbb{E}_{\xi_k}[\|\Delta_{k'}^{(m')}\|^2] + \frac{\alpha C_f M^3}{2} \sum_{m'=1}^M \mathbb{E}_{\xi_k}[\|\Delta_k^{(m')}\|^2] \\
& \leq -\frac{\alpha}{2}\|\nabla f(W_k)\|^2 + \alpha^2 L_f \sigma^2 + \frac{\alpha C_f M^2}{2} \sum_{m'=1}^M \sum_{k'=k-(M-m'+1)}^{k-1} \mathbb{E}_{\xi_k}[\|\Delta_{k'}^{(m')}\|^2] \\
& \quad - \frac{\alpha C_f M^2}{2} \sum_{m'=1}^M \sum_{k'=k-(M-m'+1)}^{k-1} \mathbb{E}_{\xi_k}[\|\Delta_{k'}^{(m')}\|^2] + \alpha^3 C_f M^3 \sigma^2 \\
& \quad - \left(\frac{1}{4\alpha} - \alpha C_f M^3 \right) \mathbb{E}_{\xi_k}[\|W_{k+1} - W_k + \alpha(\nabla f(W_k; \xi_k) - \nabla f(W_k))\|^2] \\
& \leq -\frac{\alpha}{2}\|\nabla f(W_k)\|^2 + \alpha^2 L_f \sigma^2 + \alpha^3 C_f M^3 \sigma^2
\end{aligned}$$

where the fourth inequality holds because

$$\begin{aligned}
\sum_{m'=1}^M \mathbb{E}_{\xi_k}[\|\Delta_k^{(m')}\|^2] &= \sum_{m'=1}^M \mathbb{E}_{\xi_k}[\|W_{k+1}^{(m')} - W_k^{(m')}\|^2] \\
&= \mathbb{E}_{\xi_k}[\|W_{k+1} - W_k\|^2] \\
&\leq 2\mathbb{E}_{\xi_k}[\|W_{k+1} - W_k + \alpha(\nabla f(W_k; \xi_k) - \nabla f(W_k))\|^2] \\
&\quad + 2\alpha^2 \mathbb{E}_{\xi_k}[\|\nabla f(W_k; \xi_k) - \nabla f(W_k)\|^2] \\
&\leq 2\mathbb{E}_{\xi_k}[\|W_{k+1} - W_k + \alpha(\nabla f(W_k; \xi_k) - \nabla f(W_k))\|^2] + 2\alpha^2 \sigma^2. \quad (101)
\end{aligned}$$

and the last inequality is earned by letting $\alpha \leq \sqrt{\frac{1}{4C_f M^3}}$. Reorganizing the terms yield

$$\frac{\alpha}{2}\|\nabla f(W_k)\|^2 \leq \mathbb{V}_k - \mathbb{E}_{\xi_k}[\mathbb{V}_{k+1}] + \alpha^2 L_f \sigma^2 + \alpha^3 C_f M^3 \sigma^2.$$

Therefore, by telescoping and taking the expectation, we get

$$\begin{aligned} \frac{1}{K} \sum_{k=0}^{K-1} \mathbb{E}[\|\nabla f(W_k)\|^2] &\leq \frac{2(\mathbb{V}_0 - \mathbb{E}[\mathbb{V}_K])}{\alpha K} + 2\alpha L_f \sigma^2 + 2\alpha^2 C_f M^3 \sigma^2 \\ &\leq \frac{2(f(W_0) - f^*)}{\alpha K} + 2\alpha L_f \sigma^2 + 2\alpha^2 C_f M^3 \sigma^2. \end{aligned}$$

Letting $\alpha \leq \sqrt{\frac{f(W_0) - f^*}{L_f \sigma^2 K}}$, we obtain that

$$\frac{1}{K} \sum_{k=0}^{K-1} \mathbb{E}[\|\nabla f(W_k)\|^2] \leq 4\sqrt{\frac{(f(W_0) - f^*)L_f \sigma^2}{K}} + \frac{2C_f M^3 (f(W_0) - f^*)}{KL_f}.$$

The proof is completed. \square

G Simulation details

This section provides details about the experiments in Section 5. The analog training algorithm, i.e., Analog SGD, is provided by the open-source simulation toolkit AIHWKIT [31], which has Apache-2.0 license; see github.com/IBM/aihwkit. We use *Softbound* device provided by AIHWKIT to simulate the asymmetric linear device (ALD), by setting its upper and lower bound as τ . The digital algorithm, including SGD, and datasets used in this paper, including CIFAR10 and CIFAR-100, are provided by PYTORCH, which has BSD license; see <https://github.com/pytorch/pytorch>.

The other setting follows the standard settings of AIHWKIT, including output noise (0.5 % of the quantization bin width), quantization and clipping (output range set 20, output noise 0.1, and input and output quantization to 8 bits). Noise and bound management techniques are used in [33]. A learnable scaling factor is set after each analog layer, which is updated using digital SGD.

Compute Resources. We conduct our simulations on an NVIDIA RTX 3090 GPU, which has 24GB memory. The simulations take from 30 minutes to 7 hours, depending on the size of the model and the dataset.

Statistical Significance. The simulations reported in Figure 2 and 4 are repeated three times. The randomness originates from the data shuffling, random initialization, and random noise in the analog device simulator. The mean and standard deviation are calculated from the final output of each run using *NumPy* library.

layer name	output size	10-layer	34-layer
conv1	112×112	7×7, 64, stride 2	
		3×3 max pool, stride 2	
conv2_x	56×56	$\begin{bmatrix} 3 \times 3, 64 \\ 3 \times 3, 64 \end{bmatrix} \times 1$	$\begin{bmatrix} 3 \times 3, 64 \\ 3 \times 3, 64 \end{bmatrix} \times 3$
conv3_x	28×28	$\begin{bmatrix} 3 \times 3, 128 \\ 3 \times 3, 128 \end{bmatrix} \times 1$	$\begin{bmatrix} 3 \times 3, 128 \\ 3 \times 3, 128 \end{bmatrix} \times 4$
conv4_x	14×14	$\begin{bmatrix} 3 \times 3, 256 \\ 3 \times 3, 256 \end{bmatrix} \times 1$	$\begin{bmatrix} 3 \times 3, 256 \\ 3 \times 3, 256 \end{bmatrix} \times 6$
conv5_x	7×7	$\begin{bmatrix} 3 \times 3, 512 \\ 3 \times 3, 512 \end{bmatrix} \times 1$	$\begin{bmatrix} 3 \times 3, 512 \\ 3 \times 3, 512 \end{bmatrix} \times 3$
fc	1×1	average pool, fully connected, softmax	
block number		6	18

Table 3: ResNet models in the simulations. Downsampling is performed by conv3_1, conv4_1, and conv5_1 with a stride of 2.

Image classification on CIFAR10/CIFAR100 with Resnet models. In the simulations, we train ResNet models on two benchmark datasets: CIFAR-10 and CIFAR-100. The CIFAR-10 dataset consists of 60,000 32×32 color images across 10 classes, with each class representing a distinct category such as airplanes, cars, and birds. The CIFAR-100 dataset is similar in format but includes 100 classes.

In Figure 4 and 5, ResNet10 is chosen while in Figure 1, a larger model, ResNet34 is chosen. As Table 3 shows, ResNet10 and ResNet34 are composed of 6 and 18 blocks, respectively. In Figure 4 and 5, each stage contains one block while in Figure 1, 18 blocks are separated into $M = 1, 2, 4, 8, 12, 16$ stages as evenly as possible.

Each model was trained over 300 epochs using a mini-batch size of $B_{\text{mini}} = 128$ and micro-batch-size $B_{\text{micro}} = 16$ by default. The initial learning rate of $\alpha = 0.1$ was employed, while for Resnet34 with stage number $M = 12, 16$, the initial learning rate is $\alpha = 0.01$. The transfer learning rate of Tiki-Taka is chosen to be equal to the initial learning rate and kept fit during the training. The learning rate α was reduced by a factor of 10 every 100 epochs. To further enhance the model's ability to generalize across diverse images, we applied data augmentation techniques such as random cropping, horizontal flipping, and color jittering [34].